

AD _____

Award Number: W81XWH-07-1-04J1

TITLE: V^•cā * Á@Á } &[* ^} &Á^|çæ &Á -Á^||Áæ@•ā } Áæ á& q •\^|çæÁ^} ^•Á
æ^&c áÁ^ ÁÖPÇá^|çā } •Á Á|ææ &Á

PRINCIPAL INVESTIGATOR: Ö:ÄÜ& áÚ[, ^!•

CONTRACTING ORGANIZATION: Ô[|áÁ] |ā * Áæà[|Áæ[|æ[|
Ô[|áÁ] |ā * Áæà[|ÄYÁFÍ G Á

REPORT DATE: Jul^ ÁÇF€

TYPE OF REPORT: Øā æ

PREPARED FOR: U.S. Army Medical Research and Materiel Command
Fort Detrick, Maryland 21702-5012

DISTRIBUTION STATEMENT: Approved for public release; distribution unlimited

The views, opinions and/or findings contained in this report are those of the author(s) and should not be construed as an official Department of the Army position, policy or decision unless so designated by other documentation.

REPORT DOCUMENTATION PAGE				Form Approved OMB No. 0704-0188	
Public reporting burden for this collection of information is estimated to average 1 hour per response, including the time for reviewing instructions, searching existing data sources, gathering and maintaining the data needed, and completing and reviewing this collection of information. Send comments regarding this burden estimate or any other aspect of this collection of information, including suggestions for reducing this burden to Department of Defense, Washington Headquarters Services, Directorate for Information Operations and Reports (0704-0188), 1215 Jefferson Davis Highway, Suite 1204, Arlington, VA 22202-4302. Respondents should be aware that notwithstanding any other provision of law, no person shall be subject to any penalty for failing to comply with a collection of information if it does not display a currently valid OMB control number. PLEASE DO NOT RETURN YOUR FORM TO THE ABOVE ADDRESS.					
1. REPORT DATE (DD-MM-YYYY) 01-07-2010		2. REPORT TYPE Final		3. DATES COVERED (From - To) 1 JUL 2007 - 30 JUN 2010	
4. TITLE AND SUBTITLE Testing the oncogenic relevance of cell adhesion and cytoskeletal genes affected by DNA deletions in breast cancer				5a. CONTRACT NUMBER	
				5b. GRANT NUMBER W81XWH-07-1-0495	
				5c. PROGRAM ELEMENT NUMBER	
6. AUTHOR(S) Dr. Scott Powers E-Mail: powers@cshl.edu				5d. PROJECT NUMBER	
				5e. TASK NUMBER	
				5f. WORK UNIT NUMBER	
7. PERFORMING ORGANIZATION NAME(S) AND ADDRESS(ES) Cold Spring Harbor Laboratory Cold Spring Harbor, NY 11724				8. PERFORMING ORGANIZATION REPORT NUMBER	
9. SPONSORING / MONITORING AGENCY NAME(S) AND ADDRESS(ES) U.S. Army Medical Research and Materiel Command Fort Detrick, Maryland 21702-5012				10. SPONSOR/MONITOR'S ACRONYM(S)	
				11. SPONSOR/MONITOR'S REPORT NUMBER(S)	
12. DISTRIBUTION / AVAILABILITY STATEMENT Approved for Public Release; Distribution Unlimited					
13. SUPPLEMENTARY NOTES					
14. ABSTRACT There are numerous genomic alterations that occur in breast cancer and most other commonly occurring epithelial cancers, but we still don't have a complete understanding of which of the hundreds of altered genes are actually doing something to cause or maintain cancer progression. It is important to have a complete understanding so that we can design more effective therapies. In this project we have used functional assays to test the oncogenic function of genes that are commonly altered in human cancer including cytoskeletal and cell adhesion genes. We discovered that CYFIP1, a subunit of the WAVE complex, which regulates cytoskeletal dynamics, is commonly deleted in breast cancer and has tumor suppressor function (Silva et al., Cell 2009 137:1047). We also discovered that TSPAN31, a cell adhesion gene that is amplified in diverse cancers including sarcomas and breast cancer, is a functional oncogene (Sawey et al., Cancer Cell 2011 19:347). These results establish that genomic alteration of cytoskeletal and cell adhesion genes play a functional role in tumor progression and this suggests new strategies for treatment.					
15. SUBJECT TERMS oncogenes/tumor suppressor genes/breast cancer/cytoskeleton					
16. SECURITY CLASSIFICATION OF:			17. LIMITATION OF ABSTRACT	18. NUMBER OF PAGES	19a. NAME OF RESPONSIBLE PERSON
a. REPORT	b. ABSTRACT	c. THIS PAGE			USAMRMC
U	U	U	UU	35	19b. TELEPHONE NUMBER (include area code)

Table of Contents

Introduction	Page 4
Body	Pages 4 – 8
Key Research Accomplishments	Page 8
Reportable Outcomes	Page 8
Conclusion	Pages 8 - 9
References	Page 9
Appendices (copies of PDFs of published papers)	

INTRODUCTION

Many human oncogenes and tumor suppressors are directly involved in mitogenic signaling or apoptosis, but over the past several years, in part due to the increased awareness of the importance of changes in cellular architecture and invasive properties in cancer cells, scientists have come to appreciate the potential oncogenic significance of genes directly involved in cell adhesion and the cytoskeleton. The aim of this study was therefore to directly test the oncogenic properties of certain cytoskeletal and/or cell adhesion genes. These particular genes were picked because they were determined that they were genomically altered in human cancer, and thus potential “driver” genes that could, if validated, represent new therapeutic targets or suggest new therapeutic strategies.

BODY: Completion of this project resulted in the publication of two publications in top-tier journals (Silva, Ezhkova et al. 2009; Sawey, Chanrion et al. 2011). The three specific tasks in the approved Statement of Work were to (1) to construct tools to alter the expression of candidate cancer genes belonging to the cytoskeletal/cell adhesion category, (2) use these tools to test the oncogenic significance of these genes, and (3) test the role of select genes in migration and invasion assays. Each one of these tasks has been completed, as detailed below.

We begin this project, we used high-resolution profiling of DNA copy number alterations with the ROMA platform to detect focal deletions (< 2Mb) in a panel of 293 primary human cancers and 71 cancer cell lines. More than 90% of these samples were

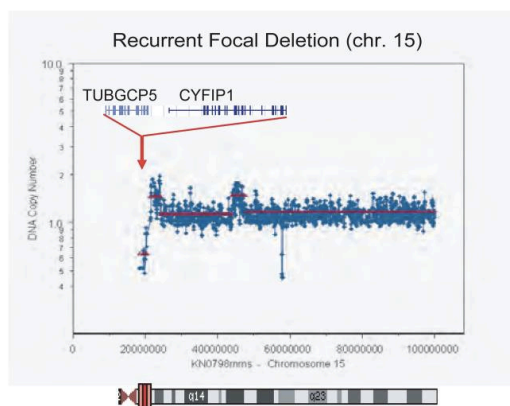


Figure 1. Representative focal deletion found on chromosome 15 in a cancer sample, affecting the cytoskeletal gene *CYFIP1*. The genes shown correspond to the consensus epicenter of the deletion (red area in the chromosome ideogram).

from common epithelial tumor types, including 83 lung, 104 breast, and 71 colon cancers. Of 36 regions identified using our criteria, 10 harbored genes previously shown to be homozygously deleted in cancer, including *RB1*, *PTEN*, *CDK2N*, *SMAD4/DPC4*. We also detected 24 focally deleted loci that did not contain any known tumor suppressor but did contain cytoskeletal and cell adhesion genes (Silva, Ezhkova et al. 2009).

To test the oncogenic significance of these genes, we used MCF-10A which is an immortalized but not transformed

mammary epithelial cell line that forms 3D acinar structures when grown on extracellular matrix components (ECM, matrigel). This model recreates aspects of epithelial cellular organization that occur in tissues more than do classical 2D cultures.

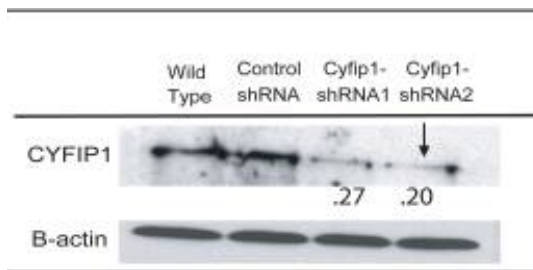


Figure 2. Level of Cyfip1 silencing in the MCF-10A cells analyzed by Western blotting.

Alterations in several oncogenes or tumor suppressors involved in proliferation, polarization or apoptosis disturb normal acinar architecture, resulting in overtly abnormal morphologies that can be easily observed (Muthuswamy, Li et al. 2001). Focusing on focal deletions without known tumor suppressors and including cytoskeletal and cell adhesion genes, we used stable shRNA expression to create cell lines in which twenty nine of the thirty five genes located in these regions were silenced to varying degrees (Figure 2) (Silva, Ezhkova et al. 2009). These lines were individually tested in the 3D morphogenesis assay. Although the majority of shRNA-expressing MCF-10A derivatives produced acini with a normal appearance, cells expressing shRNAs against *CYFIP1* generated abnormal structures (Figure 3). 20% of knock-down acini appeared as shapeless or oval structures instead of the normal symmetrical spheres (<5% in control acini; T-test, $p < .01$).

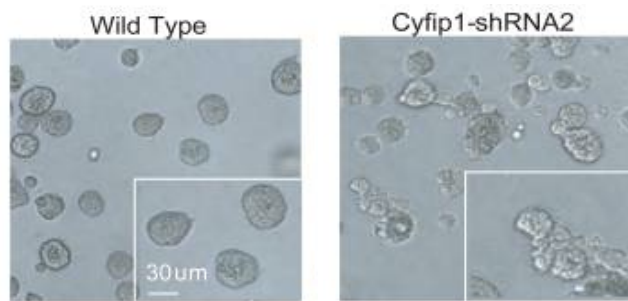


Figure 3. Morphology of the acini formed by control cells (wild type and control shRNA) and Cyfip1 knock-down MCF-10A cells.

This phenotype was reproduced using two distinct Cyfip1 shRNAs (Figure 2). We also showed that knockdown of Cyfip1 disrupted cell adhesion by altering E-cadherin distribution and disturbing focal adhesion complexes (Silva, Ezhkova et al. 2009). Finally, we showed that Cyfip1 directly affects invasion in vivo and that its loss of function cooperates

with RAS oncogene activation to induce malignancy (Silva, Ezhkova et al. 2009).

Cyfip1 is a Rac-1 interacting cytoskeletal protein, which transmits signals from Rac-1 to the ARP2/3 complex by modulating the activity of the Wasp family member, Wave, within the WAVE complex. Wave-mediated activation of ARP2/3 induces the nucleation of G-actin to form a membrane protrusion at the leading edge of cells

growing in classical two-dimensional (2D) cultures, called a lamellipodium (Hall 1998; Jaffe and Hall 2003). Although the function of the WAVE complex in site-directed actin polymerization and membrane protrusion formation is well characterized, it was unclear whether distortion of this process could influence tumorigenesis. Our data indicate that Cyfip1 can impact tumorigenesis through its effects on cytoskeletal dynamics and cell-cell and cell-substratum adhesion.

We also constructed expression cDNA vectors to test the function of candidate oncogenes belonging to the cytoskeletal/cell adhesion category (Sawey, Chanrion et al. 2011). *TSPAN31* encodes a member of the tetraspanin family of cell surface receptors and was first identified as a gene (*SAS*, for Sarcoma Amplified Sequence) that is invariably co-amplified with *CDK4* in human sarcomas (Jankowski, Mitchell et al. 1994). Although the precise biochemical function of *TSPAN31* isn't known, the related tetraspanin CD9 is a cell-surface protein that associates with integrin adhesion receptors and regulates integrin-dependent cell migration and invasion (Powner, Kopp et al. 2011). We showed that overexpression of either *CDK4* or *TSPAN31* could induce tumorigenicity in a transplantable hepatocyte liver cancer model (Sawey, Chanrion et al. 2011). Furthermore, we have recently found that *TSPAN31* acts as a

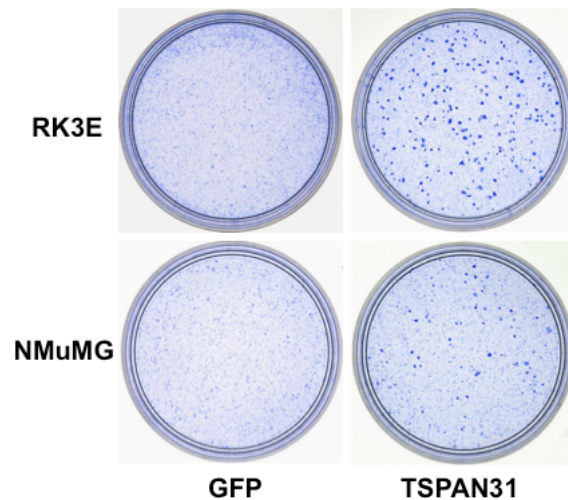


Figure 4. Foci formation induced after two weeks following transfection with either control empty (GFP) vector or by a *TSPAN31* cDNA expression vector.

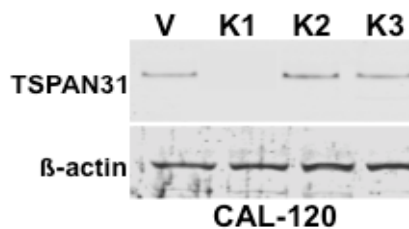


Figure 5. Level of *TSPAN31* silencing in the CAL-120 cells analyzed by Western blotting.

classic oncogene in its ability to induce morphologically dense foci in two different immortalized non-tumorigenic cells (Figure 4). Additionally, we have used the BIOPREDSi algorithm to design three shRNA sequences targeting *TSPAN31* (Huesken, Lange et al. 2005), and have found one hairpin that is effective in knocking down expression of *TSPAN31* in the breast cancer cell line CAL-120 which harbors a *TSPAN31/CDK4* amplicon (Figure 5).

In preliminary experiments, we have determined that the single effective shRNA construct targeting *TSPAN31* can significantly inhibit the growth of CAL-120 (30% reduction in growth rate, $p < 0.01$) and dramatically suppress the growth of HT1080, a sarcoma cell line that expresses high levels of *TSPAN31* (85% growth inhibition, $p < 0.001$).

KEY RESEARCH ACCOMPLISHMENTS:

- Validation of the cytoskeletal gene *CYFIP1* as a tumor suppressor invasion gene
- Validation of the cell adhesion gene *TSPAN31* as a human oncogene

REPORTABLE OUTCOMES:

- Silva, J. M., Ezhkova, E., Silva, J., Heart, S., Castillo, M., Campos, Y., Castro, V., Bonilla, F., Cordon-Cardo, C., Muthuswamy, S. K., **Powers, S.**, Fuchs, E. and Hannon, G. J. 2009. Cyfip1 is a putative invasion suppressor in epithelial cancers. *Cell* 137: 1047-1061.
- Sawey, E. T., Chanrion, M., Cai, C., Wu, G., Zhang, J., Zender, L., Zhao, A., Busuttil, R. W., Yee, H., Stein, L., French, D. M., Finn, R. S., Lowe, S. W. and Powers, S. 2011. Identification of a therapeutic strategy targeting amplified FGF19 in liver cancer by oncogenomic screening. *Cancer Cell* 19: 347-358.

CONCLUSION: We have found that two cytoskeletal/ cell adhesion genes, *CYFIP1* and *TSPAN31*, are genetically altered in human cancers by changes in DNA copy number, and have provided strong evidence that these genetic alterations directly contribute to

cancer progression. While the translational impact of the *CYFIP1* results may take years of work and much deeper understanding of the cytoskeletal network, *TSPAN31* is a cell surface protein that would be amenable to monoclonal antibody inhibition. Based on our preliminary results with RNAi indicating that inhibition of *TSPAN31* has anti-cancer properties, we have initiated a project to develop monoclonal antibodies to the extracellular domain of TPSPAN31.

REFERENCES:

- Hall, A. 1998. Rho GTPases and the actin cytoskeleton. *Science* **279**: 509-514.
- Huesken, D., Lange, J., Mickanin, C., Weiler, J., Asselbergs, F., Warner, J., Meloon, B., Engel, S., Rosenberg, A., Cohen, D., Labow, M., Reinhardt, M., Natt, F. and Hall, J. 2005. Design of a genome-wide siRNA library using an artificial neural network. *Nat Biotechnol* **23**: 995-1001.
- Jaffe, A. B. and Hall, A. 2003. Cell biology. Smurfing at the leading edge. *Science* **302**: 1690-1691.
- Jankowski, S. A., Mitchell, D. S., Smith, S. H., Trent, J. M. and Meltzer, P. S. 1994. SAS, a gene amplified in human sarcomas, encodes a new member of the transmembrane 4 superfamily of proteins. *Oncogene* **9**: 1205-1211.
- Muthuswamy, S. K., Li, D., Lelievre, S., Bissell, M. J. and Brugge, J. S. 2001. ErbB2, but not ErbB1, reinitiates proliferation and induces luminal repopulation in epithelial acini. *Nat Cell Biol* **3**: 785-792.
- Powner, D., Kopp, P. M., Monkley, S. J., Critchley, D. R. and Berditchevski, F. 2011. Tetraspanin CD9 in cell migration. *Biochem Soc Trans* **39**: 563-567.
- Sawey, E. T., Chanrion, M., Cai, C., Wu, G., Zhang, J., Zender, L., Zhao, A., Busuttil, R. W., Yee, H., Stein, L., French, D. M., Finn, R. S., Lowe, S. W. and Powers, S. 2011. Identification of a therapeutic strategy targeting amplified FGF19 in liver cancer by Oncogenomic screening. *Cancer Cell* **19**: 347-358.
- Silva, J. M., Ezhkova, E., Silva, J., Heart, S., Castillo, M., Campos, Y., Castro, V., Bonilla, F., Cordon-Cardo, C., Muthuswamy, S. K., Powers, S., Fuchs, E. and Hannon, G. J. 2009. Cyfip1 is a putative invasion suppressor in epithelial cancers. *Cell* **137**: 1047-1061.

Cyfp1 Is a Putative Invasion Suppressor in Epithelial Cancers

Jose M. Silva,^{1,6} Elena Ezhkova,² Javier Silva,³ Stephen Heart,¹ Mireia Castillo,⁴ Yolanda Campos,⁵ Veronica Castro,^{1,6} Felix Bonilla,³ Carlos Cordon-Cardo,⁴ Senthil K. Muthuswamy,¹ Scott Powers,¹ Elaine Fuchs,² and Gregory J. Hannon^{1,*}

¹Watson School Biological Sciences, Howard Hughes Medical Institute, Cold Spring Harbor Laboratory,

1 Bungtown road, Cold Spring Harbor, NY 11724, USA

²Howard Hughes Medical Institute, The Rockefeller University, 1230 York Avenue, New York, NY 10065, USA

³Puerta de Hierro Hospital, Genetic Oncology Department, San Martín de Porres n° 4, Madrid 28035, Spain

⁴Herbert Irving Comprehensive Cancer Center, Columbia University, 1130 St. Nicholas Avenue, New York, NY 10032, USA

⁵Virgen de la Salud Hospital, Pathology Department, Barber 30, Toledo 45004, Spain

⁶Present address: Institute for Cancer Genetics, Herbert Irving Comprehensive Cancer Center, Columbia University, 1130 St. Nicholas Avenue, New York, NY 10032, USA

*Correspondence: hannon@cshl.edu

DOI 10.1016/j.cell.2009.04.013

SUMMARY

Identification of bona fide tumor suppressors is often challenging because of the large number of genetic alterations present in most human cancers. To evaluate candidate genes present within chromosomal regions recurrently deleted in human cancers, we coupled high-resolution genomic analysis with a two-stage genetic study using RNA interference (RNAi). We found that *Cyfp1*, a subunit of the WAVE complex, which regulates cytoskeletal dynamics, is commonly deleted in human epithelial cancers. Reduced expression of CYFIP1 is commonly observed during invasion of epithelial tumors and is associated with poor prognosis in this setting. Silencing of *Cyfp1* disturbed normal epithelial morphogenesis in vitro and cooperated with oncogenic Ras to produce invasive carcinomas in vivo. Mechanistically, we have linked alterations in WAVE-regulated actin dynamics with impaired cell-cell adhesion and cell-ECM interactions. Thus, we propose *Cyfp1* as an invasion suppressor gene.

INTRODUCTION

Development of technologies that scan the genome, such as expression profiling (Fan et al., 2006; Trevino et al., 2007), analysis of copy number variations (Firestein et al., 2008; Hicks et al., 2006), or massively parallel sequencing (Campbell et al., 2008; Chiang et al., 2009), has provided us with the potential to molecularly profile the entire set of genetic alterations present in human cancers. However, the inability to discriminate which of these myriad genetic variations causally contribute to tumorigenesis remains a major barrier.

The use of RNAi to attenuate the expression of candidate genes represents a powerful strategy to link genotype to phenotype. To examine the impact of silencing candidates within

regions of deletion in human tumors, we chose to use a three-dimensional (3D) culture model that recapitulates many aspects of epithelial morphogenesis in vitro (Debnath et al., 2003; Fischbach et al., 2007).

By coupling genomic and genetic analysis, we have identified *Cyfp1* as a potential tumor suppressor that regulates invasive behavior. CYFIP1 is a RAC1-interacting protein (Kobayashi et al., 1998), which transmits signals from RAC1 to the ARP2/3 complex by modulating the activity of the WASP family members, WAVE1–3, within the WAVE complex. WAVE-mediated activation of ARP2/3 induces the nucleation of G-actin to form a membrane protrusion, called a lamellipodium, at the leading edges of cells growing in classical two-dimensional (2D) cultures (Kunda et al., 2003; Stradal et al., 2004; Takenawa and Suetsugu, 2007). Although the function of the WAVE complex in site-directed actin polymerization and membrane protrusion formation is well characterized, it was unclear whether distortion of this process could influence tumorigenesis. Our data indicate that CYFIP1 can impact tumorigenesis through its effects on cytoskeletal dynamics and cell-cell and cell-substratum adhesion. These studies also provide a general path toward identifying underlying driver mutation in regions of genetic aberration in human cancers.

RESULTS

CYFIP1 Is a Regulator of Epithelial Morphogenesis that Is Altered in Tumors

We used high-resolution profiling of DNA copy number alterations (Hicks et al., 2006) to detect focal deletions (<2 Mb) in a panel of 293 primary human cancers and 71 cancer cell lines (S.P., unpublished data). More than 90% of these samples were from common epithelial tumor types, including 83 lung, 104 breast, and 71 colon cancers. Of 36 regions identified using our criteria, 10 harbored genes previously shown to be homozygously deleted in cancer, including *Rb1*, *Pten*, *Cdk2n*, *Smad4*, *Dpc4* (Ikediobi et al., 2006), *Lrp1b*, *Fhit*, *Park2*, *Wwox* (Smith et al., 2007), miR-16/miR-15 (Calin et al., 2002), and *Runx1* (Silva

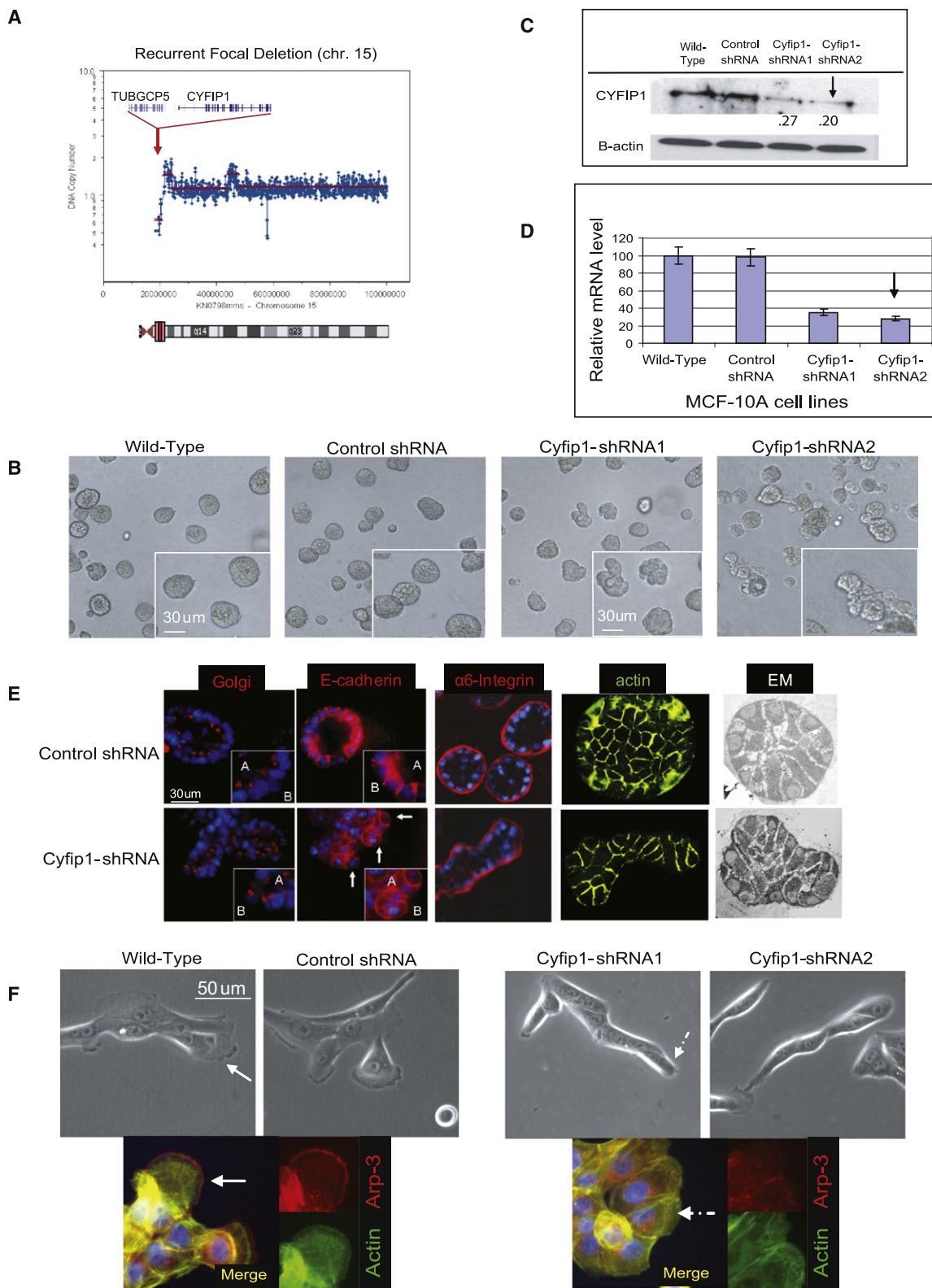


Figure 1. ROMA Deletion Profile of *Cyfip1* and Effect of Knockdown on Morphogenesis

(A) Representative focal deletion found on chromosome 15 in a lung cancer sample. The genes shown correspond to the consensus epicenter of the deletion (red area in the chromosome ideogram).

et al., 2003). Two additional loci contained candidate tumor suppressor genes with observed bi-allelic point mutations, including the activin A type II receptor (*Acvr2*) (Hempen et al., 2003) and the phosphatase *Ptpr* (Wang et al., 2004). We also detected 24 focally deleted loci that did not contain any known tumor suppressor (Table S1 available online, Figure 1A).

MCF-10A is an immortalized but not transformed mammary epithelial cell line that forms 3D acinar structures when grown on extracellular matrix components (ECM, matrigel). This model recreates aspects of epithelial cellular organization that occur in tissues more than classical 2D cultures do. Alterations in several oncogenes or tumor suppressors involved in proliferation, polarization, or apoptosis disturb normal acinar architecture, resulting in overtly abnormal morphologies that can be easily observed (Debnath et al., 2003; Muthuswamy et al., 2001).

Focusing on focal deletions without known tumor suppressors, we used stable shRNA expression to create cell lines in which 29 of the 35 genes located in these regions were silenced to varying degrees (Table S1). These lines were individually tested in the 3D morphogenesis assay. Although the majority of shRNA-expressing MCF-10A derivatives produced acini with a normal appearance, cells expressing shRNAs against *Cyfp1* generated abnormal structures (Figure 1B). Twenty percent of knockdown acini appeared as shapeless or oval structures instead of the normal symmetrical spheres (<5% in control acini; t test, $p < .01$). This phenotype was reproduced using several distinct *Cyfp1* shRNAs, and its severity correlated with the degree of *Cyfp1* knockdown (Figures 1C and 1D).

Although knockdown acini formed hollow lumens, they were smaller than those formed in controls due to the transition from spherical to oval shape (Figure 1E). Examination of structural markers (Debnath et al., 2003) revealed that a majority of the cells in the knockdown acini maintained basal ($\alpha 6$ -integrin) and lateral (E-cadherin) polarization and the apical/basal organization of the golgi and nuclei. Interestingly, it was common to find individual cells that had broken out the acinar architecture. These cells displayed a less cubical, more spherical shape with abnormally intense basal E-cadherin staining and a random positioning of the golgi/nucleus. All of these characteristics were suggestive of polarization defects (Figure 1E). Importantly, while wild-type acini presented an almost perfect symmetry, a disorganized and chaotic distribution was present in knockdown acini (Figure 1E). Finally, we did not find significant differences in the levels of proliferation (Ki67) or apoptosis (activated caspase-3) in knockdown acini (data not shown). As expected, *Cyfp1* knockdown cells grown in standard 2D culture conditions did not form lamellipodia (Figure 1F).

Alteration of *Cyfp1* in Human Cancers

Since *Cyfp1* loss could alter acinar morphology, implicating it as a potential tumor suppressor, we examined a set of 841 addi-

tional human tumors where we cataloged both focal and larger deletions affecting the *Cyfp1* locus. This revealed frequent alteration of *Cyfp1* in epithelial tumors (Table S2). Most often, losses appeared to be heterozygous and affected most of 15q, although focal deletions affecting smaller regions were also observed (Figure 1A). Importantly, a significant correlation existed between DNA copy number and *Cyfp1* expression for all tumor types examined (Table S2).

Frequently, the accumulation of genetic and/or epigenetic alterations in a tumor suppressor leads to loss of its expression. Immunohistochemistry showed robust CYFIP1 staining in the epithelium in human tissues (Figure 2A). In contrast, an examination of 249 tumor samples representing four of the most common human epithelial tumor types (breast, colon, lung, and bladder) indicated that loss of expression of CYFIP1 (defined as fewer than 10% positive tumor cells) was a common event. Up to 63% of lung (32/51) (Figure 2B), 31% of breast (22/70) (Figure 2C), 59% of colon (39/66) (Figure 2D), and 24% of bladder (15/62) (Figure 2E) cancers had negative staining. Importantly, 100% superficial bladder carcinomas (noninvasive) were CYFIP1 positive (30/30) and displayed strong staining (80% of samples had more than 40% positive cells), whereas 47% of invasive bladder tumors (15/32) were negative ($p = 1.65 \times 10^{-5}$). It is also notable that 75% of breast metastases analyzed (Figure 2C) were CYFIP1 negative (3/4). Additionally, we analyzed two ductal carcinoma in situ (DCI) of the breast where normal ducts were surrounding the tumor lesion (Figure 2C). This gave us the possibility of directly comparing the dysplastic cells with their normal counterparts. Although DCI lesions were positive for CYFIP1 staining, they did show a clear reduction in the staining as compared to normal ducts.

Globally, our results suggest that loss of CYFIP1 expression correlates with tumor progression in epithelial cancers and raise the possibility that loss of CYFIP1 might correlate with clinical outcome. We therefore examined by quantitative RT-PCR (QRT-PCR) the expression of *Cyfp1* in an additional 170 human tumors (84 colons and 86 breasts) with available histological and pathological data (see Supplemental Experimental Procedures). In order to select a metric to stratify tumor samples in a way comparable to our immunohistochemistry, we first selected 8 tumors with different expression levels of *Cyfp1* (from very low to high) that also had available matched paraffin sections. We compared QRT-PCR and immunohistochemistry data to generate a standard curve (Figure S1). Through this approach, we found that low expression of *Cyfp1* (negative tumors) was significantly ($p < 0.05$) associated with higher stage. This also ($p < 0.1$) correlated with lymph node metastases in invasive ductal breast carcinomas (IDC). In colon cancers, low expression of *Cyfp1* was significantly associated with vascular invasion and correlated with higher stage (Table S3). It was therefore critical to probe mechanisms by which loss of *Cyfp1* might contribute to tumorigenesis.

(B) Morphology of the acini formed by control cells (wild-type and control shRNA) and *Cyfp1* knockdown MCF-10A cells.

(C) Level of *Cyfp1* silencing in the MCF-10A cells analyzed by western blotting and (D) quantitative RT-PCR (QRT-PCR). Error bars show standard deviation from the mean ($n = 3$). The arrow indicates the shRNA selected for further studies.

(E) Characterization of acinar architecture by Immunofluorescence and electromicroscopy (EM).

(F) Morphology of the cells from (B) when grown in classical 2D cultures. The IF presents the same cells staining with Arp-3, a canonical marker of lamellipodia and actin (Boguslavsky et al., 2007). Lamellipodial structures are indicated by continuous arrows; lack of lamellipodia is indicated by discontinuous arrows.

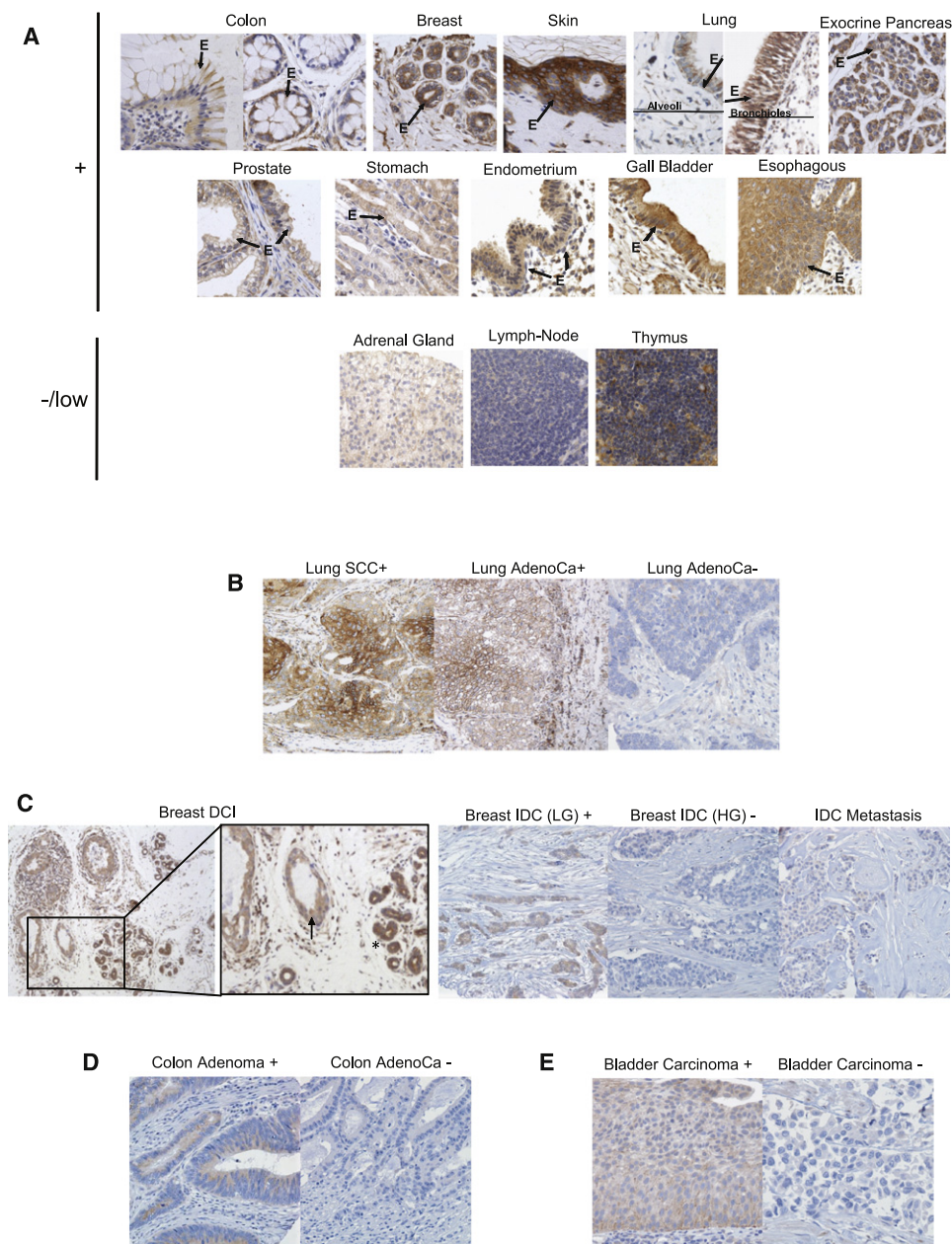


Figure 2. CYFIP1 Expression in Human Normal and Tumor Tissues and Its Association with Tumor Progression

Representative figures of CYFIP1 expression detected by immunohistochemistry (IH) in (A) normal tissues. The “E” and the arrows indicate the epithelium.

(B) The majority of lung squamous cell carcinomas (SCC) and some adenocarcinomas (AdenoCa) showed a membranous-cytoplasmic expression of the protein (+), while most lung adenocarcinomas were found to have a negative phenotype (–).

(C) Left panels show a ductal carcinoma in situ of the breast (DCI) (arrow) together with normal ducts (asterisk). Right panels show that low-grade (LG) invasive ductal breast carcinoma (IDC) exhibited intense and homogenous staining of CYFIP1, while most high-grade (HG) IDC and bone metastatic adenocarcinoma lesions revealed a negative phenotype.

(D) In colon tumor samples, high-grade noninvasive adenomas maintain CYFIP1 while it is lost in a majority of invasive adenocarcinoma.

(E) In bladder tumor samples, we observed that all low-grade noninvasive superficial bladder carcinomas displayed a positive phenotype, while the majority of high-grade invasive bladder carcinomas revealed undetectable CYFIP1 levels.

CYFIP1 Regulates Epithelial Morphogenesis as Part of the WAVE Complex

In addition to its role as a component of WAVE, CYFIP1 interacts with FMR1, an RNA-binding protein (Billuart and Chelly, 2003).

Although its function in that context is poorly understood, various observations suggest that it affects local protein translation and/or transport (Zalfa et al., 2006). We set out to determine whether our observed phenotypes were mediated by defects in actin

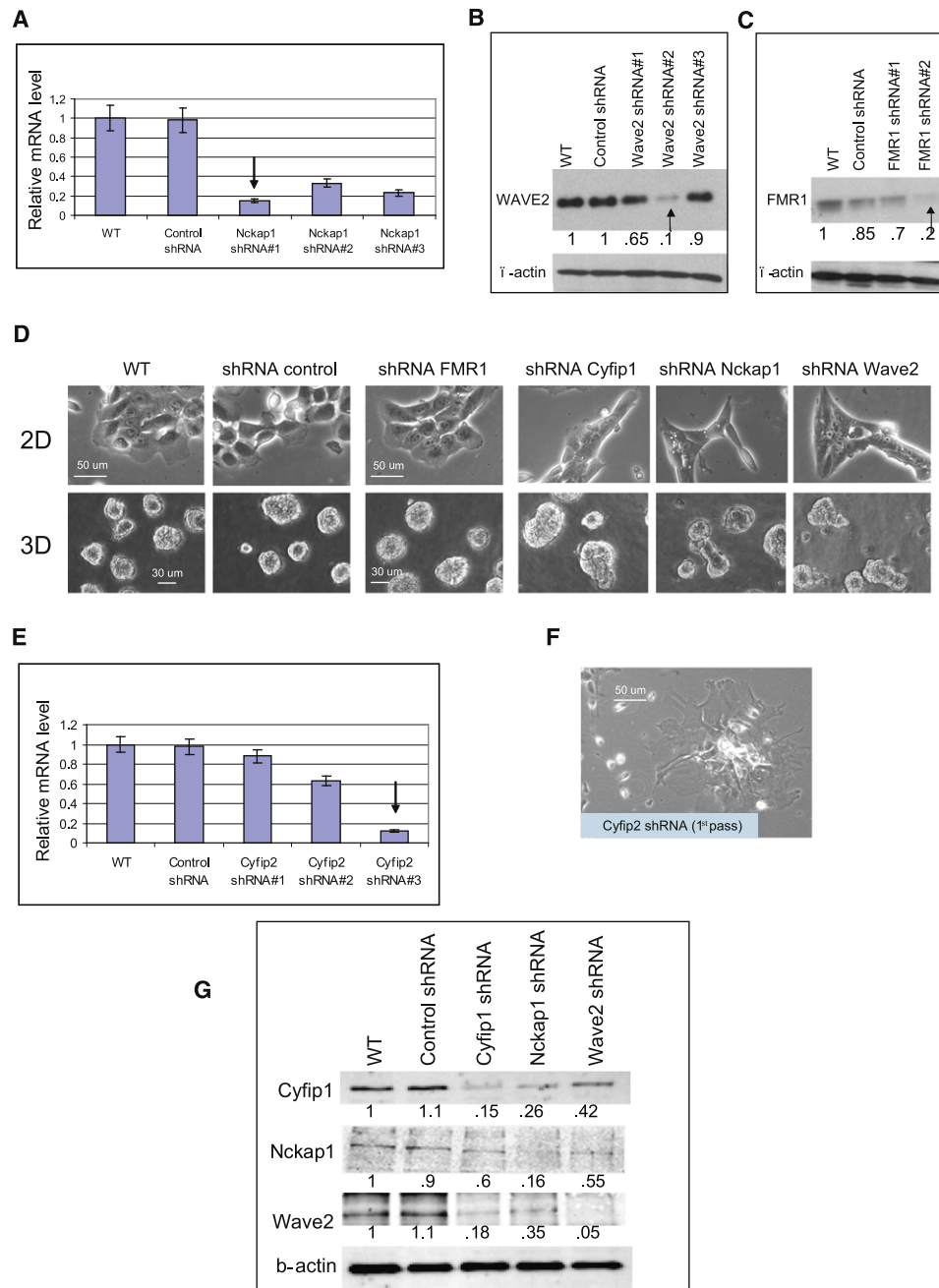


Figure 3. Silencing of WAVE Complex Components Phenocopies the Knockdown of Cyfip1

(A–C) Level of specific gene silencing in MCF-10A cells from (D) analyzed by western blotting or QRT-PCR.

(D) Representative morphologies of FMR1 and WAVE component knockdown cells growing in 2D and 3D culture.

(E) Level of Cyfip2 silencing in MCF-10A. The arrow indicates the shRNA selected for further studies.

(F) Representative picture of the phenotype generated in 2D cultures after silencing of Cyfip2.

(G) Western blots show the steady-state protein levels of CYFIP1, NCKAP1, and WAVE2 after individual WAVE components were silenced. The numbers inside the western blot are the quantitative values of the bands normalized to the wild-type.

In (A) and (E), error bars show standard deviation from the mean (n=3).

remodeling (WAVE pathway), by alterations in mRNA metabolism (FMR1 pathway), or by both. ShRNAs targeting core components of the two pathways were selected (Figures 3A–

3C) and stably expressed in MCF-10A cells to produce knock-down lines. Suppression of FMR1 did not produce any evident difference in 2D colonies or 3D acinar structures. In contrast,

knockdown of WAVE pathway components, *Nckap1* and *Wave2*, generated phenotypes similar to those observed upon *Cyfp1* silencing (Figure 3D). The phenotype seen in *Nckap1* knockdown cells was exceptionally penetrant, with almost 100% of colonies in 2D lacking lamellipodia (t test, $p < .01$) and 50%–70% (t test, $p < .01$) of acini displaying abnormal morphologies (Figure S2A). To verify the specificity of the observed phenotypes we transduced WAVE knockdown cells with a nontargeted form of the mouse *Cyfp1* homolog. This rescued the formation of lamellipodia in *Cyfp1* but not in *Nckap1* knockdown cells (Figures S2B–S2D).

Cyfp1 is highly conserved through evolution. In humans, two homologs, *Cyfp1* and *Cyfp2*, share 88% amino acid sequence identity (Schenck et al., 2001). Interestingly, RNAi of *Cyfp2* (Figure 3E) induced abnormal spreading of MCF-10A cells (Figure 3F) and a dramatic reduction in proliferation (Figures S3A and S3B). Consequently, *Cyfp2* was not studied further.

Silencing any WAVE component destabilizes the complex, leading to proteasome-mediated degradation of the other subunits (Innocenti et al., 2004; Kunda et al., 2003). We also observed this phenomenon in cultured MCF-10A cells (Figure 3G) and in vivo in subcutaneous tumors formed in nude mice by injecting oncogene-transformed MCF-10A cells carrying different WAVE shRNAs (Figure S4).

Three WAVE family members (WAVE1–3) are present in the mammalian genome (Takenawa and Suetsugu, 2007). Their individual knockdown has been reported to increase the steady-state levels of others family members, possibly as a compensatory mechanism (Zipfel et al., 2006). We noted a similar effect in our *Wave2* knockdown cells (Figure S3C). Overall, these results suggest that interference with the WAVE complex and its function in regulating actin dynamics leads to the phenotypes similar to those generated by suppression of *Cyfp1*.

These data support the hypothesis that CYFIP1 might contribute to tumor suppression through its role in the WAVE complex. In accord with this notion, our ROMA analyses revealed that deletions of *Wave2* were also present in human cancers, although the *Nckap1* locus was highly stable (Table S4). We therefore set out to understand precisely how changes in WAVE activity might impact critical hallmarks of cancer cells.

Suppression of WAVE Disrupts Cell Adhesion by Altering E-Cadherin Distribution

Uncontrolled proliferation and increased resistance to stress stimuli are two hallmarks of cancer cells (Hanahan and Weinberg, 2000). WAVE knockdown cells showed no significant difference in short-term growth in 2D or 3D cultures (Figures S4A and S4B) in comparison to control cells. These results agree with our previous finding that the level of Ki67 was unchanged in matrigel-cultured *Cyfp1* knockdown acini. Moreover, knockdown cells behaved similarly to controls during loss of anchorage (anoikis) or growth factor starvation (Figures S4C and S4D).

MCF-10A cells are not tumorigenic, but they can be transformed by strong oncogenic stimuli (Datta et al., 2007). To test whether the growth of MCF-10A cells is affected in an in vivo setting by compromising WAVE activity, we knocked down WAVE components in normal or oncogene-transformed MCF-10A cells

(overexpressing a constitutively active form of ErbB2, MCF-10A/ErbB2) and injected these into nude mice. These experiments revealed that disruption of the WAVE pathway neither transformed wild-type MCF-10A cells nor altered the growth of transformed MCF-10A/ErbB2 as subcutaneous xenografts (Figures S4E and S4F). Xenograft tumors were of high grade but showed no remarkable differences between controls and knockdowns. This result was not exclusive to MCF-10A cells, as silencing of *Nckap1* did not alter the ability of three other tumorigenic breast cancer lines (MCF-7, T-47D, and MDA-MB-231) to form subcutaneous tumors in immunocompromised mice (Figure S4G, data not shown).

Along with a balance between proliferation and cell death, epithelial tissue homeostasis is enforced by its characteristic architecture (Hanahan and Weinberg, 2000; Perez-Moreno et al., 2003), and distortion of this organization, induced by defects in cell adhesion, is often associated with epithelial tumorigenesis (Shin et al., 2006). Therefore, we tested whether knocking down WAVE components had any effect on cell-cell and cell-substratum adhesion.

MCF-10A cells were plated on plastic and grown to confluence for 48 hr; in this scenario they form a typical epithelial sheet wherein the cells are tightly bound to each other by a variety of adhesion complexes and junctions (Underwood et al., 2006). Next, EDTA was added in order to chelate calcium, an essential modulator of cadherin-mediated cell-cell adhesion, and changes in the morphology of the culture were recorded by live imaging. After 1 hr, control cells started losing cell-cell adhesion and showed fewer surface contacts, though they still maintained significant interactions at this time point (Movies S1A and S1B; Figure 4A). In contrast, EDTA treatment of MCF-10A cells engineered to have reduced cell adhesion capacity (overexpressing Snail) resulted in rapid rounding of cells and loss of almost all cell-cell contacts (Movie S1C; Figure 4A). WAVE knockdown cells also lost cell-cell adhesion more rapidly than controls (Movies S1D–S1F; Figure 4A). To obtain a more quantitative measurement of this defect we performed cell aggregation assays (Willemeyer et al., 2002). Here, the percentage of individual cells in suspension that form aggregates through time reflects their ability to form cell-cell contacts. Again, knockdown cells presented a significant reduction ($p < .01$) in the number of aggregates formed after 3 hr (Figure 4B).

To investigate the mechanisms underlying reduced adhesion, we examined the localization of the key adherence junction component, E-cadherin. As expected, E-cadherin accumulated along cell-cell boundaries in control cells. In contrast, knockdown of WAVE subunits generated very compacted colonies with a more diffuse pattern of staining in the cells located at the margins (Figure 4C). In fact, 2D orthogonal projections showed that E-cadherin was more spread between overlapping areas of neighboring cells (Figure S5A). This pattern changed near the center of the colonies. Here, it was common to see very intense E-cadherin signals (Figure S5B). Remarkably, DAPI staining of the colonies showed that knockdown cell nuclei commonly overlap, revealing that the cells had in fact piled on top of each other (Figure S5C). To unify these observations we monitored the growth of our engineered MCF-10A variants (Movies S2A–S2D). We found that colonies of wild-type cells

formed by an orchestrated series of events in which the cells first divide and then spread apart from each other. This process is controlled by lamellipodia-mediated motility at the periphery of the colony. Knockdown cells divided normally but were unable to separate because of the absence of lamellipodia. This, in turn, led to the formation of a mass of highly compacted cells.

During immortalization and transformation of cultured cell lines, like MCF-10A, normal actin organization and formation of adhesion contacts become aberrant (Vasioukhin et al., 2000). Low-passage keratinocytes represent an elegant and well-characterized model that more closely maintains the epithelial characteristics of normal epidermis (Vaezi et al., 2002; Vasioukhin et al., 2000). Briefly, when mouse keratinocytes are grown in media containing low calcium concentrations, they display low levels of cell-cell interaction and high motility. Increased calcium concentrations induce actin cytoskeleton remodeling that is essential to promote contacts between neighboring cells. These are eventually stabilized by cadherin-mediated intercellular adhesion. Thus, upon calcium switch, filopodia-like projections emerge between neighboring cells and become decorated with E-cadherin to generate characteristic structures called adhesion zippers. With the passage of time an increasing number of E-cadherin puncta accumulate at the zippers, which then form a continuous line at cell borders. Finally, keratinocytes polarize forming a honeycombed network of thick cortical actin belts and E-cadherin complexes in the apical plane and fluid membranes with less organized E-cadherin structures at the basal plane.

Using the keratinocyte model, we analyzed the formation of cell contacts and E-cadherin distribution after silencing the mouse homologs of *Cyfp1* and *Nckap1* (Figures S5D and S5E). As expected, at low calcium concentrations, silencing of WAVE components compromised the formation of lamellipodia (Movies S3A, S3B, and S5F). After calcium switch, control cells followed the normal pattern of adhesion (Movie S4A; Figures 4D, 4E, and S5G). Knockdown keratinocytes presented only finger-like protrusions that did not efficiently form stable interactions (Movie S4B), and numerous but transient contacts between neighboring cells predominated. This correlated with reduced E-cadherin immunostaining and fewer adhesion zippers (Figures 4D and S5G). At 8 hr after calcium exposure, a wider distribution of E-cadherin complexes and a more diffuse actin staining were observed in knockdowns as compared to controls (Figures 4D and S5G). Finally, at later time points (16 hr), 2D orthogonal and 3D projections showed that in normal keratinocytes, E-cadherin coexists with a cortical actin ring in the apical part of cells. In contrast, knockdown keratinocytes presented a patched and diffuse distribution of actin and E-cadherin with a scattered overlap between them (Figure 4E). Ultrastructural studies at this latest time point provided more detailed information. We noted that the mature architecture, normally characterized by the alignment of alternating adherence junctions (AJ) and desmosomes along sealed membranes, was replaced in knockdown cells by immature desmosomes with fewer AJ. Importantly, this led to large gaps and spaces between closely opposed keratinocytes, (Figures 4F and S5H).

We obtained cellular fractions from keratinocytes grown in low and high calcium to study the distribution of actin and

E-cadherin. We found that, in control keratinocytes, cytosolic G-actin is mobilized to the cytoskeleton (F-actin) in the presence of calcium, and this correlates temporally with the enrichment of E-cadherin in the membrane fraction (Figure 4G). These data are consistent with the immunofluorescence (IF) results, where first thick bundles filopodia and then a cortical ring of actin are formed while E-cadherin accumulates at cell-cell contacts. In knockdown cells grown in low calcium media, a substantially larger amount of actin was found unpolymerized in the cytosol (Figure 4G). After calcium switch, actin was still mobilized to the cytoskeletal fraction; however, this occurred to a lower degree than was observed in wild-type keratinocytes. Notably, E-cadherin accumulation at the membrane was also reduced (Figure 4G).

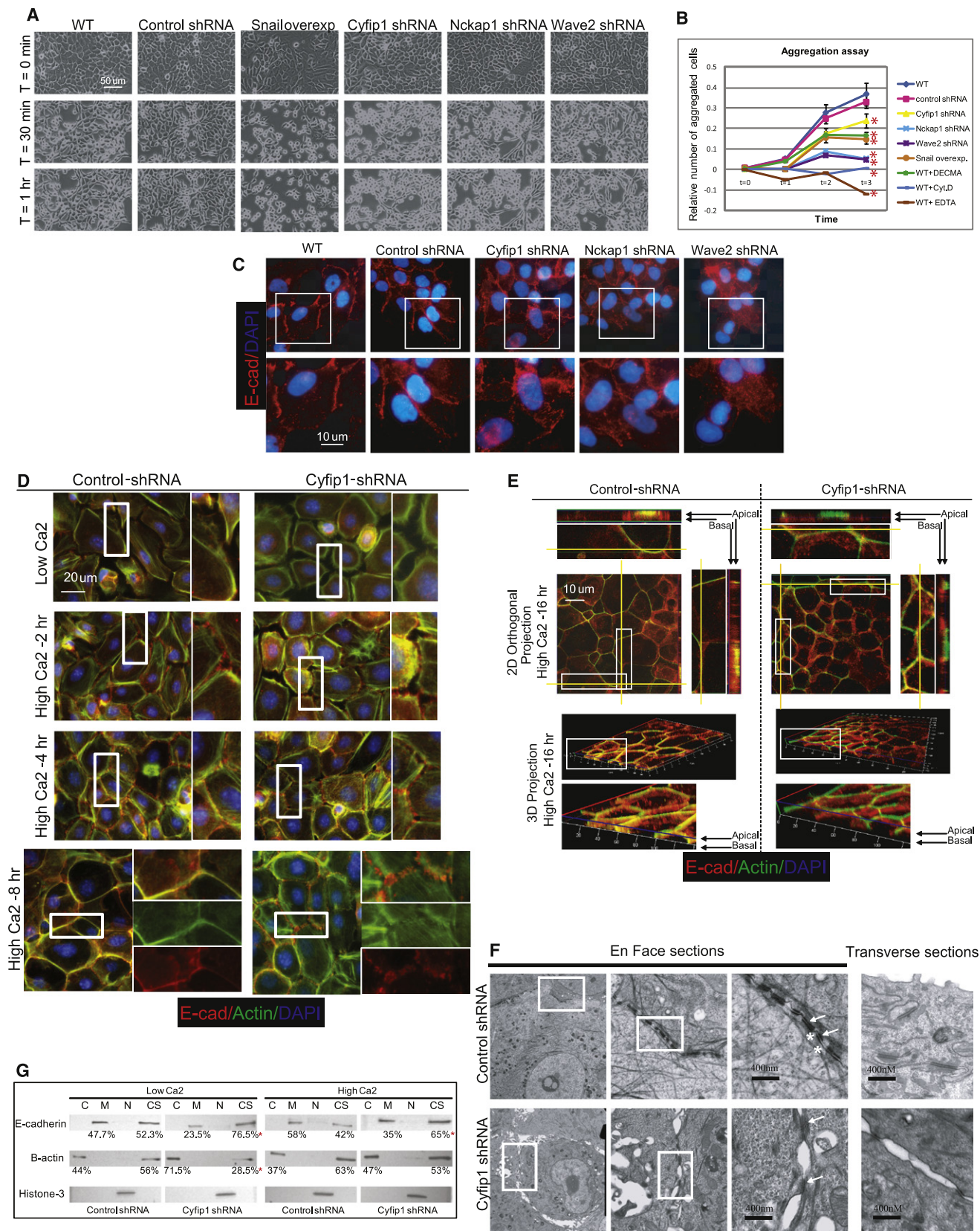
Thus, as an integrated model to explain the defects observed in WAVE-deficient cells, we propose that a lack of WAVE activity reduces the formation of AJ by reducing the formation and stabilization of filopodia-like structures and the accumulation of E-cadherin complexes at cell-cell boundaries. This physically compromises the drawing together of opposing cell surfaces, leaving the passive formation of desmosomes (Vasioukhin et al., 2000) as the only event that clamps two opposing membranes. As a result, the entire epithelial architecture fails to assemble properly. In accord with this model, silencing of WAVE components recapitulated the phenotype observed when AJ formation was compromised by α -catenin knockout or by perturbing VASP/Mena function (Vasioukhin et al., 2000). It is interesting to note that in our knockdown cells VASP localized normally at adhesion zippers (Figure S5I). However, as expected, its maturation toward a more continuous honeycomb-like belt failed.

To generate knockdown cells, we used viral transduction to produce pooled cell populations. Thus, different degrees of knockdown can be expected in individual cells, depending upon viral integration sites and copy number. IF staining of CYFIP1 in our pooled cells revealed that approximately 10% of cells still retained high expression levels, and these cells retained the ability to normally relocate E-cadherin upon calcium switch (Figure S5J). Moreover, expression of exogenous *Cyfp1* rescued the phenotype induced by silencing of the endogenous protein (Figure S5K).

Compromising WAVE Reduces Epithelial Cell-ECM Adhesion by Disturbing Focal Adhesion Complexes

MCF-10A WAVE knockdown cells also displayed an obvious defect in their ability to attach to standard tissue culture plates. Even 6 hr after plating, the majority of cells were still rounded and showed very little spreading (Figure 5A). Coating plates with Collagen-I, Collagen-IV, and Fibronectin accelerated the attachment of MCF-10A cells while no effect was observed with Laminin or Fibrinogen (Figure S6A). *Cyfp1* knockdown cells showed a pleiotropic reduction in adhesion to all tested substrates (Figures 5B–5D).

Interaction with ECM substrates is mediated by integrins, a superfamily of membrane receptors that in cultured cells are typically localized at cellular microdomains called focal adhesions (FA) (Hynes, 2002). Therefore, we assessed the status of FA formation in WAVE knockdown cells, both MCF-10A and



keratinocytes grown in low calcium medium. Control cells were well spread and displayed two morphologically different types of focal adhesions: focal contacts (robust adhesion located at the periphery) and focal complexes (smaller adhesions situated centrally). Both are characterized by the presence of markers such as Vinculin (Figures 5E and 5F) and Focal Adhesion Kinase/FAK (Figures S6B and S6C) (Hynes, 2002; Raghavan et al., 2003). In contrast, WAVE knockdown cells showed very large focal contacts at the tips of unusually thick actin cables, and the number of the internal focal complexes was substantially reduced. This phenotype mirrors that observed in integrin $\beta 1$ null (Raghavan et al., 2003) and FAK null (Schober et al., 2007) keratinocytes, where these defects were characterized as a reflection of the inability to turn over focal adhesion complexes.

WAVE Impairment Cooperates with Activated Ras to Promote Tumor Progression

To probe the relevance of our findings in an in vivo setting, we took advantage of an orthotopic mouse model that has previously been used to study links between cell adhesion and tumor progression (Dajee et al., 2003; Weinberg et al., 1991). In this model, primary keratinocytes are cotransplanted with fibroblasts onto a wounded nude mouse to reconstitute skin (Figure S7). If the keratinocytes are engineered ex vivo to express activated Ras (H-RasV12), the engrafted skin develops hyperplastic and dysplastic benign lesions (papillomas). Additional genetic alterations, such as loss of p53, permit progression to squamous cell carcinomas, which invade through the basal lamina into the dermis (Azzoli et al., 1998).

Accordingly, we found that keratinocytes that express activated Ras in combination with control shRNAs produced hyperplastic lesions in 5 out of 7 mice. In the remaining two cases, a focal area with few (1–3) individual keratinocytes invading into underlying dermis was observed. In contrast, shRNAs directed against *Cyfp1* cooperated with Ras to induce rapid progression (3–4 weeks) to squamous cell carcinoma in 6 out of 7 animals (Figure 6A). These lesions are characterized by disruption of the basal lamina as illustrated by staining with $\beta 4$ -Integrin and α -Catenin antibodies (Figure 6B). Since our silencing constructs were engineered to coexpress a fluorescent

GFP marker we could verify that cells invading and colonizing the dermal compartment were indeed those with *Cyfp1* knockdown (Figure 6C).

Reduced Expression of CYFIP1 Is Common during Tumor Invasion

During invasion of the stroma by tumor cells, the expression of many proteins changes, including adhesion molecules (e.g., E- and N-cadherin), cytoskeleton-associated proteins (e.g., Vimentin), and transcriptional regulators (e.g., Snail) (Christofori, 2006; Grunert et al., 2003). Consequently, the expression levels of these genes can serve as markers of invasion. It was therefore critical to determine whether CYFIP1 expression is also generally affected as tumor cells gain invasive potential.

To probe this possibility, we generated several mosaic mouse models (using the orthotopic transplantation previously described) that reflect different stages of tumor progression and examined the expression of CYFIP1 (Figure 7). Antibody staining revealed strong CYFIP1 expression in the epidermis that was more intense in terminally differentiated layers. In dysplastic lesions produced by the expression of oncogenic Ras, CYFIP1 was still obvious, but the lesions did not present the intense staining typical of normal, differentiated layers. When an invasive squamous cell carcinoma (SCC) was generated by silencing p53, the expression of CYFIP1 was greatly reduced at the invasive edge. Furthermore, in a more aggressive SCC generated by transplanting TGF- β -RII null keratinocytes carrying oncogenic Ras (Guasch et al., 2007), the expression of CYFIP1 was almost completely abolished in large invasive areas and coincided with a strong reduction of E-cadherin. Interestingly, we also observed reduction of CYFIP1 expression at the edges of human lung cancers (6 out of 6 comprising 3 SCC and 3 adenocarcinomas [AdenoCa.]) and breast tumors (1 out of 3 IDC) with well-defined limits between epithelial and stromal tissues (Figure S8).

We wondered whether loss of Cyfp1 expression was specific to the migratory and invasive responses that occur in tumors. We therefore tested whether changes in CYFIP1 were observed during epidermal wound healing, a nontumorigenic tissue-remodeling response. A small wound was created on

Figure 4. Silencing of WAVE Complex Components Reduces Cell-Cell Adhesion

- (A) Representative snapshot from Movies S1A–S1F after EDTA (5 mM final concentration) was added to equally confluent MCF-10A cultures.
- (B) Aggregation experiment showing the percentage of aggregates formed during 3 hr. MCF-10A cells where actin dynamics (cytochalasin-D, 1 μ g/ml) or E-cadherin-mediated adhesion (5 mM EDTA, 10 μ g/ml of DECMA E-cadherin blocking antibodies, and Snail-overexpressing cells) was abolished represent controls. Error bars show standard deviation from the mean (n=3). The red asterisks indicate p values < .05 (t test of three replicas) when the aggregation values after 3 hr were compared with wild-type cells.
- (C) Immunofluorescence showing E-cadherin and nuclear staining in controls and knockdown MCF-10A cells. Through the entire figure magnified panels represent images of the selected area (white rectangle).
- (D) Immunofluorescence showing the development of cell-cell adhesion in control and *Cyfp1* knockdown keratinocytes after calcium exposure (2, 4, and 8 hr).
- (E) Immunofluorescence of control and *Cyfp1* knockdown keratinocytes 16 hr after calcium exposure. 4 \times magnified images of selected areas together with 2D orthogonal projections (yellow lines) are shown on the side of the upper half of the figure. A 3D reconstruction of the same keratinocyte layer is shown in the lower half. 4 \times magnified images of selected areas are displayed below.
- (F) The composition shows structural studies (EM) of control and *Cyfp1* knockdown keratinocytes 16 hr after calcium switch. En face sections present three 10 \times consecutive magnifications of the same area. Arrows indicate desmosomes, and asterisks indicate adherence junctions. The transverse sections shows the apical parts of two cells from the same cultures shown en face.
- (G) Distribution of E-cadherin and B-actin in different fractions, cytoplasmic (C), membrane (M), nuclear (N), and cytoskeleton (CS) of control and *Cyfp1* knocked-down cells growing in low and high calcium media. The numbers below the blots represent the average of the quantitative value of bands in the blots from three independent experiments. The red asterisks in (B) and (G) represent p values < .05 (t test of three replicas) when the values from knockdown cells were compared with controls.

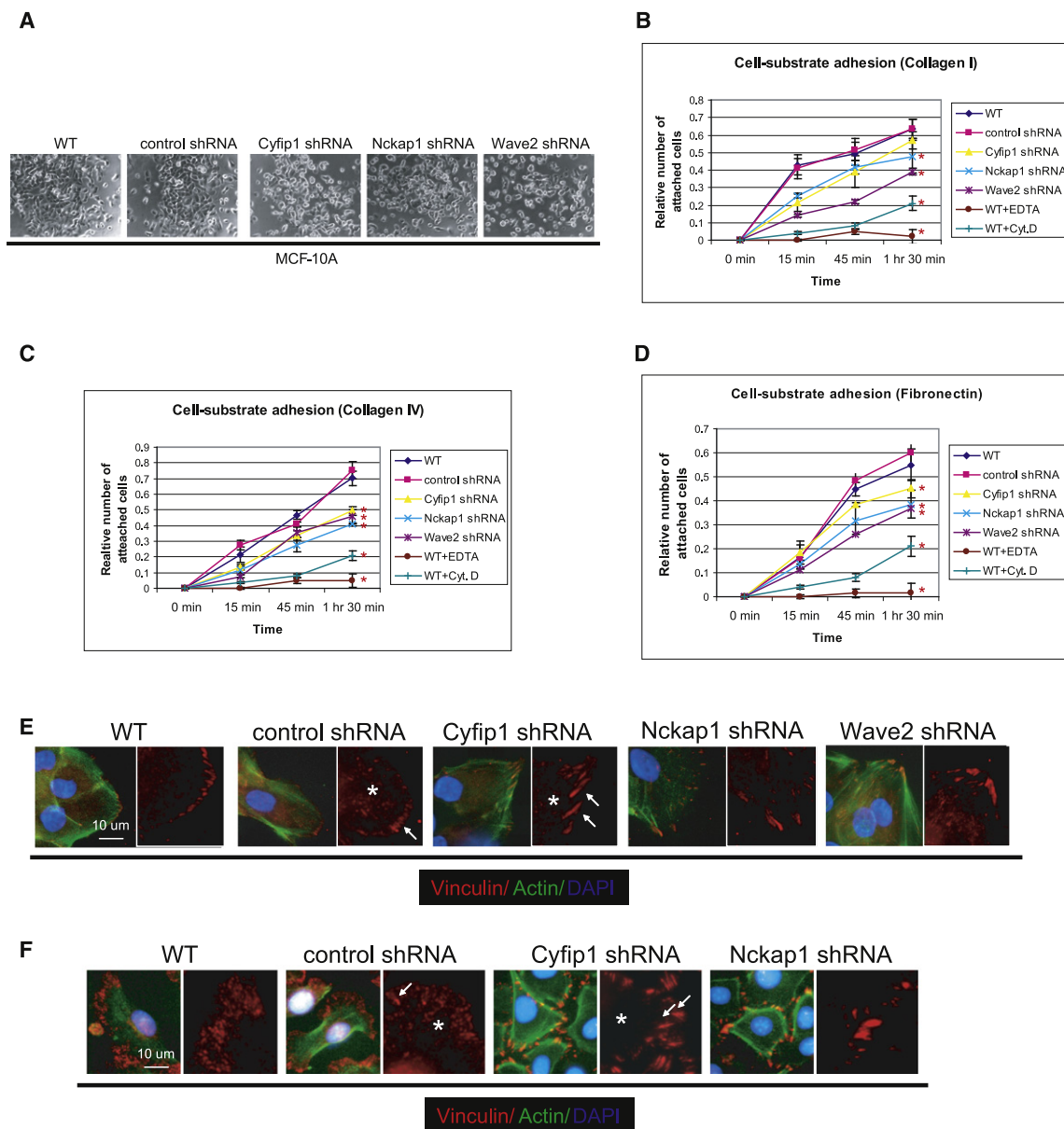


Figure 5. Silencing of WAVE Complex Components Reduces Epithelial Cell-ECM Adhesion

(A–D) Representative image of the attachment and spreading of MCF-10A WAVE knockdown cells 6 hr after plating. Kinetics of adhesion of cells from (A) in different ECM substrates, (B) Collagen-I, (C) Collagen-IV, (D) Fibronectin. As a negative control, wild-type cells were plated in the presence of 5 mM of EDTA (WT+EDTA). The graphics also show the attachment kinetics of wild-type cells in the presence of an inhibitor of actin polymerization, cytochalasin-D, 2 μ M/ml (WT+CytD). Error bars in (B), (C), and (D) show standard deviation from the mean ($n = 3$). Red asterisks indicate differences statistically significant (t test, $p < .05$) compared with WT. Notice that although the p value for *Cyfip1* knockdown in (B) is not significant, it was $< .1$.

Immunofluorescence studies showing the distribution and morphology of focal adhesions, labeled with anti-Vinculin antibody, in knockdown MCF-10A cells (E) and keratinocytes (F) are shown. The arrows indicate the focal contacts and the asterisks the focal complexes.

the back of a mouse and wound closure was analyzed 2–4 days later. Although strong proliferation and mobilization of epidermal keratinocytes occurred at the area close to the wound, IF staining revealed no changes in expression of CYFIP1 (Figure 7). This result indicates that reduction of CYFIP1 expression coincides with invasiveness rather than with motility, per se.

DISCUSSION

The ability to generate a polarized cytoskeletal network that is intricately associated with intercellular junctions allows epithelial cells to integrate tension-based movements and function coordinately within a tissue (Cau and Hall, 2005; Vaezi et al., 2002). The presence of calcium modulates the interaction of

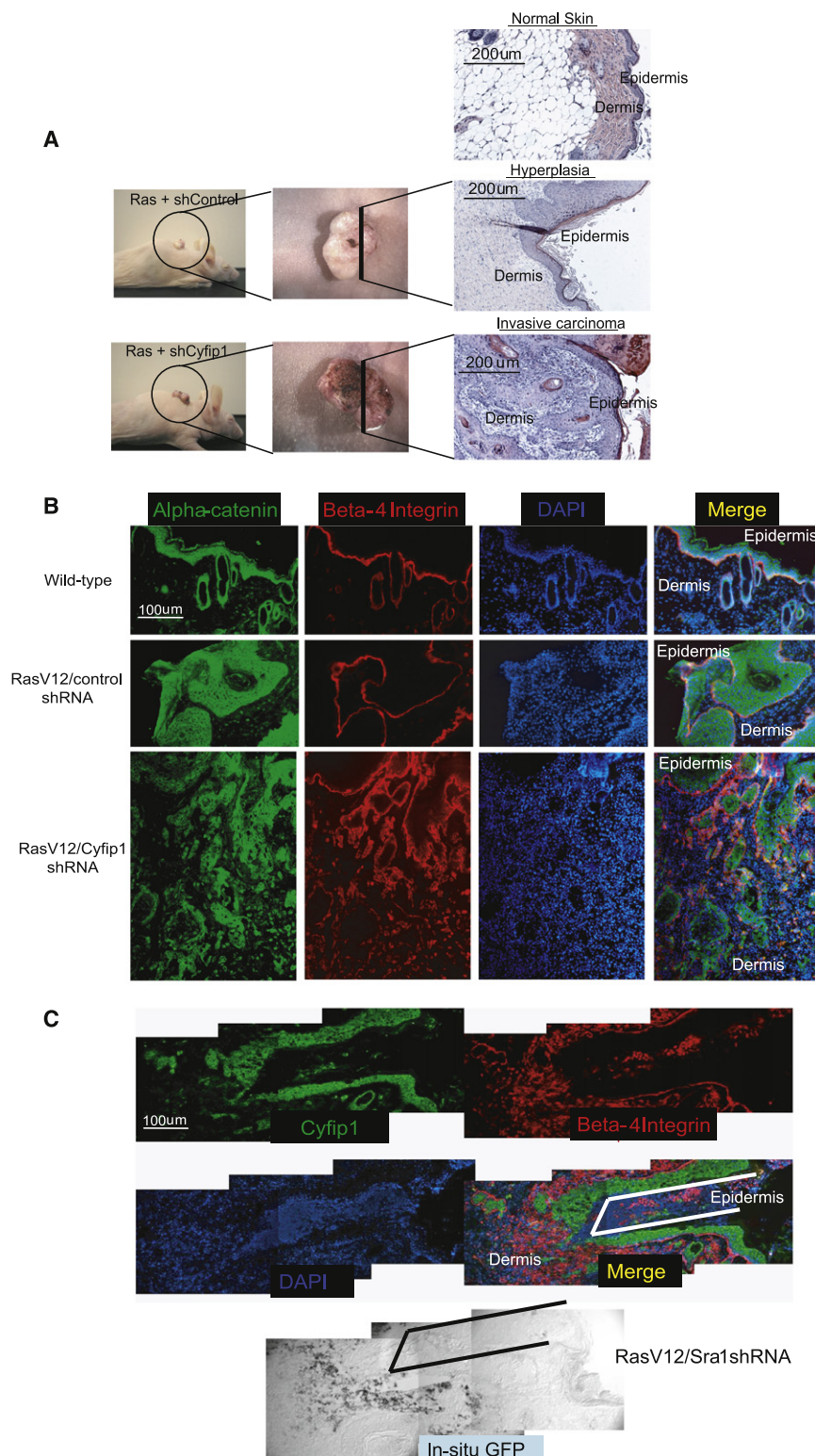


Figure 6. Knockdown of *Cyfip1* Promotes Invasion In Vivo

(A) illustrates macroscopically and microscopically the appearance of skin lesions produced in nude mice after transplantation of primary keratinocytes engineered to express oncogenic Ras or Ras plus *Cyfip1* shRNA as compared with wild-type skin. (B) Markers of the epithelial compartment of the skin (β 4-Integrin and α -Catenin) were used to study tissue architecture in sections from (A). (C) Immunofluorescence showing that invasive keratinocytes (β 4-Integrin positive) express the construct that contains the hairpin targeting CY-FIP1 (positive for GFP mRNA in the in situ panel) and show low CYFIP1 expression. The lines (black in merged panel and white in in situ panel) are used as a reference.

on the striking abnormalities that we have characterized in cells with compromised WAVE function, we propose a model wherein depletion of WAVE components directly perturbs actin dynamics, which in turn reduces epithelial adhesion and leads to disorganization of tissue architecture.

Tissue architecture represents an important level of control, which transformed cells must disrupt in order to become invasive. Correspondingly, a number of molecules that regulate tissue architecture are also commonly altered during tumor formation (e.g., E-cadherin [Cowan et al., 2005], α 6- and β 4-Integrins [Gilcrease, 2007], Podoplanin [Wicki et al., 2006], or Scribble [Bilder, 2004]). Changes in genes encoding these regulators often show a strong correlation with poor prognosis and the capacity of tumor cells to invade stromal compartments (Cowan et al., 2005; Gumbiner, 1996). We now add *Cyfip1* to those genes that modify the invasive phenotype since its suppression can promote the development of invasive carcinomas in models that would normally yield benign, noninvasive lesions.

Our observations have reinforced connections between actin dynamics and tumorigenesis, given that effects on the actin cytoskeleton impact tissue architecture and cell adhesion and consequently invasive potential. However, the catalog of downstream pathways potentially affected by disrupting WAVE may

be far from complete. Remodeling of the actin cytoskeleton influences multiple aspects of cellular behavior, including motility, adhesion, signal transduction, apoptosis, cytokinesis, endocytosis, and differentiation (Doherty and McMahon, 2008; Olson

cadherin-mediated junctions with the cytoskeleton (Gumbiner, 2005), and in some circumstances, WAVE-mediated actin reorganization has been implicated in the organization and maintenance of adhesion (Yamazaki et al., 2007). Based on this and

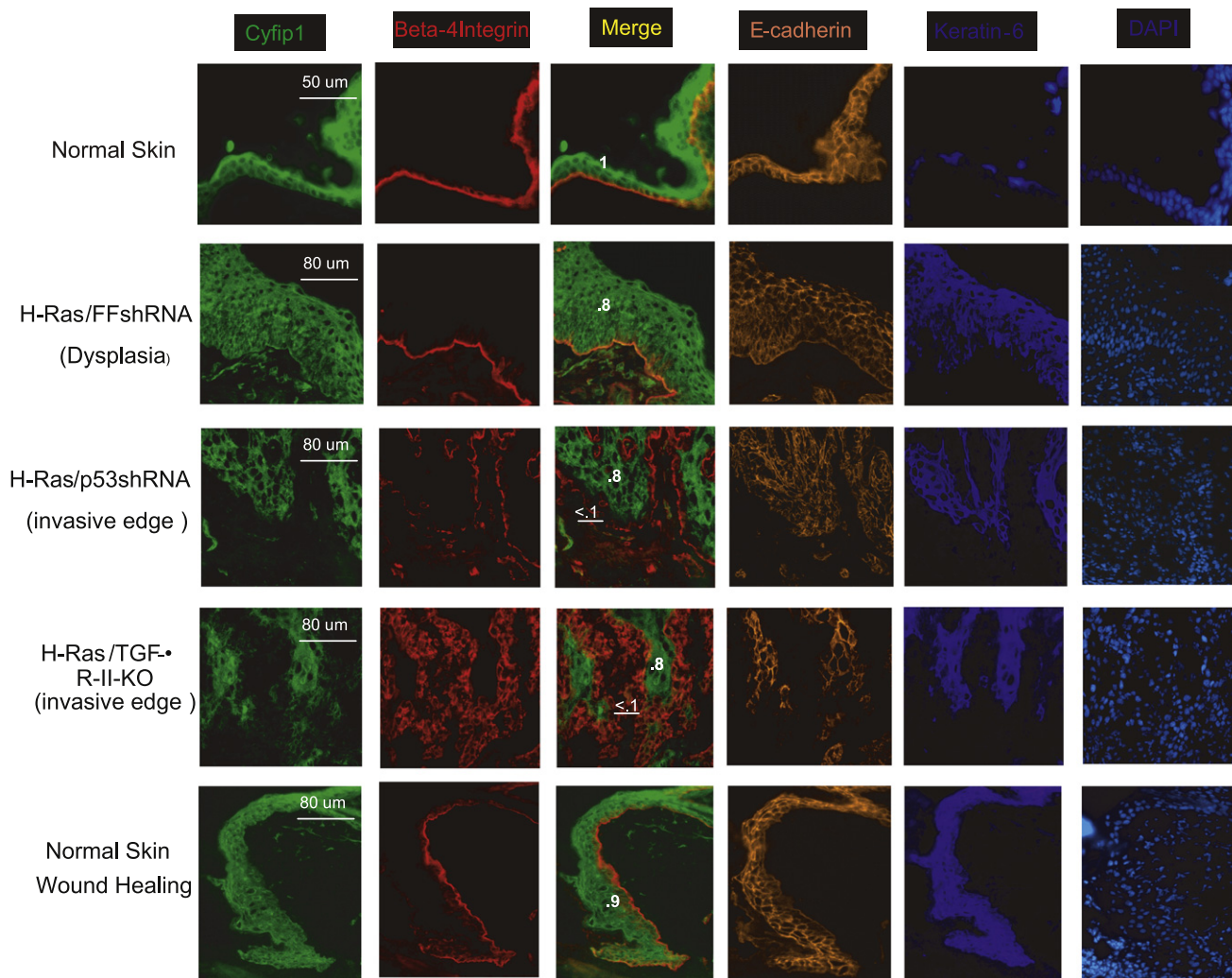


Figure 7. Downregulation of CYFIP1 Occurs during Tumor Invasion In Vivo

Immunofluorescence staining comparing the expression and distribution of CYFIP1 and different characteristic markers of the epidermis, β 4-Integrin and E-cadherin, is shown. A continuous β 4-Integrin staining is an indication of intact epidermal/dermal boundaries (normal skin, dysplasia, and wound healing). In contrast, patched and disorganized staining reflects invasion of tumor cells into the stroma (invasive edges). In this model keratin-6 is a marker that labels proliferating epidermis. Quantitative data comparing the expression of CYFIP1 at the leading edge of the invasion (underlined) and inside of the tumor (bold) are provided. The raw values were double normalized (first, internally to the staining of β 4-Integrin and then to the value of the normal skin), and these have been included in the figure.

and Sahai, 2008; Perez-Moreno et al., 2003). Thus, further work will almost certainly be required to understand the complete mechanistic basis of the effects that we observe.

A remaining critical question is whether distortion of general actin dynamics can influence epithelial tumorigenesis or whether invasive potential is impacted specifically by alterations of the WAVE/lamellipodia pathway. There are several indications that support the former hypothesis. Although cytochalasin-D was toxic, low concentrations of this drug induced abnormalities in acinar development, and specific inhibition of Rho GTPases dramatically impacted acinar architecture without compromising viability (Figure S9). Moreover, a number of genes controlling actin dynamics are altered in human

cancers (Olson and Sahai, 2008), and the formation of actin-based membrane protrusions is essential during tumor progression and invasion (Yamaguchi and Condeelis, 2007). It seems likely that there is no one unique route through which tumor cells gain the capacity to invade. Indeed, it is now clear that tumor cells are able to shift among a variety of pathways if one that fosters mobility becomes blocked (Friedl, 2004; Sanz-Moreno et al., 2008; Wolf et al., 2003). Nonetheless, our data demonstrate that alterations in either the *Cyfip1* locus or its expression contribute to the loss of epithelial cell architecture and promote tumor progression, marking this locus a strong candidate for a bona fide human invasion suppressor.

EXPERIMENTAL PROCEDURES

ROMA

High-resolution genome profiling of DNA copy number alterations was performed as previously described (Hicks et al., 2006). Focal deletions were defined as regions of less than 2 Mb.

Cell Culture and Cell Line Construction

ShRNAs cassettes from our published library (Silva et al., 2005) were cloned into a retroviral vector that links GFP to expression of the shRNA. All the available shRNAmirs targeting the same gene were pooled together to produce suppressed cell populations. The sequences for the shRNAs can be obtained at <http://codex.cshl.edu/scripts/newmain.pl> or <http://www.openbiosystems.com> and in the Supplemental Experimental Procedures. Three-dimensional cultures were performed as described previously (Debnath et al., 2003). For depletion of growth factors, all supplements were omitted from the negative media. For anoikis experiments, negative media were also used and the cells were plated on ultra low attachment plates (Packard). For cell-cell adhesion studies, 5 mM EDTA (final concentration) was added to equally confluent MCF-10A cell cultures (control and knockdown lines). For cell-ECM adhesion studies, plates coated with different ECM substrates were purchased from Cell Biolabs, and protocols recommended by the vendor were followed. All assays were done at least two independent times in triplicate.

Western Blotting, Immunofluorescence, and QRT-PCR

IF on cells seeded on glass was performed using standard methods. IF on tissue sections was performed as previously described (Kobielak and Fuchs, 2006). QRT-PCR for *Cyfp1* and *Nckap1* was done after standard total RNA extraction and reverse transcription. The antibodies, dilutions, and oligo sequences used are described in detail in the Supplemental Experimental Procedures.

Microscopy

Images of live cells were collected at 4 min intervals for 24 hr using a Zeiss observer Z1. Confocal image Z series (LSM format) were imported into the 3D module of Axiovision (version 4.6.3 Zeiss Microimaging, Thornwood, NY, USA) and maximum projection 3D images were generated. From the same Z series orthogonal perspectives were made using Zen LE (Zeiss). For standard immunofluorescence a Zeiss Axioskop 2 plus was used. For transmission electron microscopy, cells were cultured on Thermanox Nunc coverslips and then processed following the procedures described in detail in the Supplemental Experimental Procedures.

In Vivo Studies

Wild-type or knockdown cells were injected subcutaneously into nude mice, and tumor size was determined after 4–6 weeks. Engraftment experiments were performed as described previously (Azzoli et al., 1998; Weinberg et al., 1991) by infecting primary keratinocytes with retroviral constructs expressing Ha-RasV12, or different shRNAs. Mice were sacrificed and analyzed 4–5 weeks after grafting.

Human Tumor Studies

Pathological parameters are described in detail in the Supplemental Experimental Procedures. Total RNA was extracted from 30 mg of tumor samples and was reverse transcribed using standard protocols. We calculated the expression level of *Cyfp1* as the ratio: relative mRNA expression of target/relative mRNA expression of housekeeping control. The tumors were stratified based on their correlated immunohistochemistry value (explained in the main text and Figure S7). The statistical correlations were analyzed using the t test and the SPSS package.

Immunohistochemistry

Immunohistochemistry analysis was performed on formalin-fixed and paraffin-embedded tissue sections from Tissue MicroArrays (TMAs) following the standard avidin-biotin immunoperoxidase staining procedure (described in more detail in the Supplemental Experimental Procedures).

SUPPLEMENTAL DATA

Supplemental Data include Supplemental Experimental Procedures, nine figures, four tables, and four movies and can be found with this article online at [http://www.cell.com/supplemental/S0092-8674\(09\)00401-2](http://www.cell.com/supplemental/S0092-8674(09)00401-2).

ACKNOWLEDGMENTS

We are especially thankful to Victoria Aranda (CSHL) for help with the 3D model, to Alberto Muñoz (Instituto de Investigaciones Biomédicas “Alberto Sols”) for providing the Snail expression vector, and to Geraldine Guasch (Rockefeller University) for providing tissue sections of HRas/TGF- β R-II-KO mouse tumors. We also thank June Racelis for help with in situ hybridizations and Nicole Stokes for assistance with skin chamber grafting. We thank Ken Chang and Edie Davis for comments on the manuscript and for helpful discussion. This work was partially supported by the NCI with the K99/R00 project # 54010101-5411 (J.M.S.). G.J.H. and E.F. are Investigators of the Howard Hughes Medical Institute and E.E. is a Life Sciences Foundation Postdoctoral Fellow supported by the New York Stem Cell Institute. This work was supported by grants from the N.I.H (G.J.H. and E.F. R01-AR27883) and by a kind gift from Kathryn W. Davis (G.J.H.).

Received: June 29, 2008

Revised: January 23, 2009

Accepted: April 2, 2009

Published: June 11, 2009

REFERENCES

- Azzoli, C.G., Sagar, M., Wu, A., Lowry, D., Hennings, H., Morgan, D.L., and Weinberg, W.C. (1998). Cooperation of p53 loss of function and v-Ha-ras in transformation of mouse keratinocyte cell lines. *Mol. Carcinog.* 21, 50–61.
- Bilder, D. (2004). Epithelial polarity and proliferation control: links from the *Drosophila* neoplastic tumor suppressors. *Genes Dev.* 18, 1909–1925.
- Billuart, P., and Chelly, J. (2003). From fragile X mental retardation protein to Rac1 GTPase: new insights from fly CYFIP. *Neuron* 38, 843–845.
- Boguslavsky, S., Grosheva, I., Landau, E., Shtutman, M., Cohen, M., Arnold, K., Feinstein, E., Geiger, B., and Bershadsky, A. (2007). p120 catenin regulates lamellipodial dynamics and cell adhesion in cooperation with cortactin. *Proc. Natl. Acad. Sci. USA* 104, 10882–10887.
- Calin, G.A., Dumitru, C.D., Shimizu, M., Bichi, R., Zupo, S., Noch, E., Aldler, H., Rattan, S., Keating, M., Rai, K., et al. (2002). Frequent deletions and down-regulation of micro-RNA genes miR15 and miR16 at 13q14 in chronic lymphocytic leukemia. *Proc. Natl. Acad. Sci. USA* 99, 15524–15529.
- Campbell, P.J., Stephens, P.J., Pleasance, E.D., O'Meara, S., Li, H., Santarius, T., Stebbings, L.A., Leroy, C., Edkins, S., Hardy, C., et al. (2008). Identification of somatically acquired rearrangements in cancer using genome-wide massively parallel paired-end sequencing. *Nat. Genet.* 40, 722–729.
- Cau, J., and Hall, A. (2005). Cdc42 controls the polarity of the actin and microtubule cytoskeletons through two distinct signal transduction pathways. *J. Cell Sci.* 118, 2579–2587.
- Chiang, D.Y., Getz, G., Jaffe, D.B., O'Kelly, M.J., Zhao, X., Carter, S.L., Russ, C., Nusbaum, C., Meyerson, M., and Lander, E.S. (2009). High-resolution mapping of copy-number alterations with massively parallel sequencing. *Nat. Methods* 6, 99–103.
- Christofori, G. (2006). New signals from the invasive front. *Nature* 441, 444–450.
- Cowin, P., Rowlands, T.M., and Hatsell, S.J. (2005). Cadherins and catenins in breast cancer. *Curr. Opin. Cell Biol.* 17, 499–508.
- Dajee, M., Lazarov, M., Zhang, J.Y., Cai, T., Green, C.L., Russell, A.J., Marin-kovich, M.P., Tao, S., Lin, Q., Kubo, Y., et al. (2003). NF-kappaB blockade and oncogenic Ras trigger invasive human epidermal neoplasia. *Nature* 421, 639–643.

- Datta, S., Hoenerhoff, M.J., Bommi, P., Sainger, R., Guo, W.J., Dimri, M., Band, H., Band, V., Green, J.E., and Dimri, G.P. (2007). Bmi-1 cooperates with H-Ras to transform human mammary epithelial cells via dysregulation of multiple growth-regulatory pathways. *Cancer Res.* 67, 10286–10295.
- Debnath, J., Muthuswamy, S.K., and Brugge, J.S. (2003). Morphogenesis and oncogenesis of MCF-10A mammary epithelial acini grown in three-dimensional basement membrane cultures. *Methods* 30, 256–268.
- Doherty, G.J., and McMahon, H.T. (2008). Mediation, modulation, and consequences of membrane-cytoskeleton interactions. *Annu. Rev. Biophys.* 37, 65–95.
- Fan, C., Oh, D.S., Wessels, L., Weigelt, B., Nuyten, D.S., Nobel, A.B., van't Veer, L.J., and Perou, C.M. (2006). Concordance among gene-expression-based predictors for breast cancer. *N. Engl. J. Med.* 355, 560–569.
- Firestein, R., Bass, A.J., Kim, S.Y., Dunn, I.F., Silver, S.J., Guney, I., Freed, E., Ligon, A.H., Vena, N., Ogino, S., et al. (2008). CDK8 is a colorectal cancer oncogene that regulates beta-catenin activity. *Nature* 455, 547–551.
- Fischbach, C., Chen, R., Matsumoto, T., Schmelzle, T., Brugge, J.S., Polverini, P.J., and Mooney, D.J. (2007). Engineering tumors with 3D scaffolds. *Nat. Methods* 4, 855–860.
- Friedl, P. (2004). Prespecification and plasticity: shifting mechanisms of cell migration. *Curr. Opin. Cell Biol.* 16, 14–23.
- Gilcrease, M.Z. (2007). Integrin signaling in epithelial cells. *Cancer Lett.* 247, 1–25.
- Grunert, S., Jechlinger, M., and Beug, H. (2003). Diverse cellular and molecular mechanisms contribute to epithelial plasticity and metastasis. *Nat. Rev. Mol. Cell Biol.* 4, 657–665.
- Guasch, G., Schober, M., Pasolli, H.A., Conn, E.B., Polak, L., and Fuchs, E. (2007). Loss of TGFbeta signaling destabilizes homeostasis and promotes squamous cell carcinomas in stratified epithelia. *Cancer Cell* 12, 313–327.
- Gumbiner, B.M. (1996). Cell adhesion: the molecular basis of tissue architecture and morphogenesis. *Cell* 84, 345–357.
- Gumbiner, B.M. (2005). Regulation of cadherin-mediated adhesion in morphogenesis. *Nat. Rev. Mol. Cell Biol.* 6, 622–634.
- Hanahan, D., and Weinberg, R.A. (2000). The hallmarks of cancer. *Cell* 100, 57–70.
- Hempfen, P.M., Zhang, L., Bansal, R.K., Iacobuzio-Donahue, C.A., Murphy, K.M., Maitra, A., Vogelstein, B., Whitehead, R.H., Markowitz, S.D., Willson, J.K., et al. (2003). Evidence of selection for clones having genetic inactivation of the activin A type II receptor (ACVR2) gene in gastrointestinal cancers. *Cancer Res.* 63, 994–999.
- Hicks, J., Krasnitz, A., Lakshmi, B., Navin, N.E., Riggs, M., Leib, E., Esposito, D., Alexander, J., Troge, J., Grubor, V., et al. (2006). Novel patterns of genome rearrangement and their association with survival in breast cancer. *Genome Res.* 16, 1465–1479.
- Hynes, R.O. (2002). Integrins: bidirectional, allosteric signaling machines. *Cell* 110, 673–687.
- Ikedio, O.N., Davies, H., Bignell, G., Edkins, S., Stevens, C., O'Meara, S., Santarius, T., Avis, T., Barthorpe, S., Brackenbury, L., et al. (2006). Mutation analysis of 24 known cancer genes in the NCI-60 cell line set. *Mol. Cancer Ther.* 5, 2606–2612.
- Innocenti, M., Zucconi, A., Disanza, A., Frittoli, E., Areces, L.B., Steffen, A., Stradal, T.E., Di Fiore, P.P., Carlier, M.F., and Scita, G. (2004). Abi1 is essential for the formation and activation of a WAVE2 signalling complex. *Nat. Cell Biol.* 6, 319–327.
- Kobayashi, K., Kuroda, S., Fukata, M., Nakamura, T., Nagase, T., Nomura, N., Matsuura, Y., Yoshida-Kubomura, N., Iwamatsu, A., and Kaibuchi, K. (1998). p140Sra-1 (specifically Rac1-associated protein) is a novel specific target for Rac1 small GTPase. *J. Biol. Chem.* 273, 291–295.
- Kobiela, A., and Fuchs, E. (2006). Links between alpha-catenin, NF-kappaB, and squamous cell carcinoma in skin. *Proc. Natl. Acad. Sci. USA* 103, 2322–2327.
- Kunda, P., Craig, G., Dominguez, V., and Baum, B. (2003). Abi, Sra1, and Kette control the stability and localization of SCAR/WAVE to regulate the formation of actin-based protrusions. *Curr. Biol.* 13, 1867–1875.
- Muthuswamy, S.K., Li, D., Lelievre, S., Bissell, M.J., and Brugge, J.S. (2001). ErbB2, but not ErbB1, reinitiates proliferation and induces luminal repopulation in epithelial acini. *Nat. Cell Biol.* 3, 785–792.
- Olson, M.F., and Sahai, E. (2008). The actin cytoskeleton in cancer cell motility. *Clin. Exp. Metastasis* 26, 273–287.
- Perez-Moreno, M., Jamora, C., and Fuchs, E. (2003). Sticky business: orchestrating cellular signals at adherens junctions. *Cell* 112, 535–548.
- Raghavan, S., Vaezi, A., and Fuchs, E. (2003). A role for alpha1 integrins in focal adhesion function and polarized cytoskeletal dynamics. *Dev. Cell* 5, 415–427.
- Sanz-Moreno, V., Gadea, G., Ahn, J., Paterson, H., Marra, P., Pinner, S., Sahai, E., and Marshall, C.J. (2008). Rac activation and inactivation control plasticity of tumor cell movement. *Cell* 135, 510–523.
- Schenck, A., Bardoni, B., Moro, A., Bagni, C., and Mandel, J.L. (2001). A highly conserved protein family interacting with the fragile X mental retardation protein (FMRP) and displaying selective interactions with FMRP-related proteins FXR1P and FXR2P. *Proc. Natl. Acad. Sci. USA* 98, 8844–8849.
- Schober, M., Raghavan, S., Nikolova, M., Polak, L., Pasolli, H.A., Beggs, H.E., Reichardt, L.F., and Fuchs, E. (2007). Focal adhesion kinase modulates tension signaling to control actin and focal adhesion dynamics. *J. Cell Biol.* 176, 667–680.
- Shin, K., Fogg, V.C., and Margolis, B. (2006). Tight junctions and cell polarity. *Annu. Rev. Cell Dev. Biol.* 22, 207–235.
- Silva, F.P., Morolli, B., Storlazzi, C.T., Anelli, L., Wessels, H., Bezrookove, V., Kluin-Nelemans, H.C., and Giphart-Gassler, M. (2003). Identification of RUNX1/AML1 as a classical tumor suppressor gene. *Oncogene* 22, 538–547.
- Silva, J.M., Li, M.Z., Chang, K., Ge, W., Golding, M.C., Rickles, R.J., Siolas, D., Hu, G., Paddison, P.J., Schlabach, M.R., et al. (2005). Second-generation shRNA libraries covering the mouse and human genomes. *Nat. Genet.* 37, 1281–1288.
- Smith, D.I., McAvoy, S., Zhu, Y., and Perez, D.S. (2007). Large common fragile site genes and cancer. *Semin. Cancer Biol.* 17, 31–41.
- Stradal, T.E., Rottner, K., Disanza, A., Confalonieri, S., Innocenti, M., and Scita, G. (2004). Regulation of actin dynamics by WASP and WAVE family proteins. *Trends Cell Biol.* 14, 303–311.
- Takenawa, T., and Suetsugu, S. (2007). The WASP-WAVE protein network: connecting the membrane to the cytoskeleton. *Nat. Rev. Mol. Cell Biol.* 8, 37–48.
- Trevino, V., Falciani, F., and Barrera-Saldana, H.A. (2007). DNA microarrays: a powerful genomic tool for biomedical and clinical research. *Mol. Med.* 13, 527–541.
- Underwood, J.M., Imbalzano, K.M., Weaver, V.M., Fischer, A.H., Imbalzano, A.N., and Nickerson, J.A. (2006). The ultrastructure of MCF-10A acini. *J. Cell. Physiol.* 208, 141–148.
- Vaezi, A., Bauer, C., Vasioukhin, V., and Fuchs, E. (2002). Actin cable dynamics and Rho/Rock orchestrate a polarized cytoskeletal architecture in the early steps of assembling a stratified epithelium. *Dev. Cell* 3, 367–381.
- Vasioukhin, V., Bauer, C., Yin, M., and Fuchs, E. (2000). Directed actin polymerization is the driving force for epithelial cell-cell adhesion. *Cell* 100, 209–219.
- Wang, Z., Shen, D., Parsons, D.W., Bardelli, A., Sager, J., Szabo, S., Ptak, J., Silliman, N., Peters, B.A., van der Heijden, M.S., et al. (2004). Mutational analysis of the tyrosine phosphatome in colorectal cancers. *Science* 304, 1164–1166.
- Weinberg, W.C., Morgan, D.L., George, C., and Yuspa, S.H. (1991). A comparison of interfollicular and hair follicle derived cells as targets for the v-rasHa oncogene in mouse skin carcinogenesis. *Carcinogenesis* 12, 1119–1124.
- Wicki, A., Lehembre, F., Wick, N., Hantusch, B., Kerjaschki, D., and Christofori, G. (2006). Tumor invasion in the absence of epithelial-mesenchymal transition:

- podoplanin-mediated remodeling of the actin cytoskeleton. *Cancer Cell* 9, 261–272.
- Wilkemeyer, M.F., Menkari, C.E., Spong, C.Y., and Charness, M.E. (2002). Peptide antagonists of ethanol inhibition of I1-mediated cell-cell adhesion. *J. Pharmacol. Exp. Ther.* 303, 110–116.
- Wolf, K., Mazo, I., Leung, H., Engelke, K., von Andrian, U.H., Deryugina, E.I., Strongin, A.Y., Brocker, E.B., and Friedl, P. (2003). Compensation mechanism in tumor cell migration: mesenchymal-amoeboid transition after blocking of pericellular proteolysis. *J. Cell Biol.* 160, 267–277.
- Yamaguchi, H., and Condeelis, J. (2007). Regulation of the actin cytoskeleton in cancer cell migration and invasion. *Biochim. Biophys. Acta* 1773, 642–652.
- Yamazaki, D., Oikawa, T., and Takenawa, T. (2007). Rac-WAVE-mediated actin reorganization is required for organization and maintenance of cell-cell adhesion. *J. Cell Sci.* 120, 86–100.
- Zalfa, F., Achsel, T., and Bagni, C. (2006). mRNPs, polysomes or granules: FMRP in neuronal protein synthesis. *Curr. Opin. Neurobiol.* 16, 265–269.
- Zipfel, P.A., Bunnell, S.C., Witherow, D.S., Gu, J.J., Chislock, E.M., Ring, C., and Pendergast, A.M. (2006). Role for the Abi/wave protein complex in T cell receptor-mediated proliferation and cytoskeletal remodeling. *Curr. Biol.* 16, 35–46.

Identification of a Therapeutic Strategy Targeting Amplified *FGF19* in Liver Cancer by Oncogenomic Screening

Eric T. Sawey,¹ Maia Chanrion,¹ Chunlin Cai,¹ Guanming Wu,² Jianping Zhang,¹ Lars Zender,¹ Alice Zhao,³ Ronald W. Busuttill,⁴ Herman Yee,⁵ Lincoln Stein,^{1,2} Dorothy M. French,⁶ Richard S. Finn,³ Scott W. Lowe,^{1,*} and Scott Powers^{1,*}

¹Cold Spring Harbor Laboratory, Cold Spring Harbor, NY 11724, USA

²Ontario Institute for Cancer Research, Toronto, Ontario M5G 0A3, Canada

³Department of Medicine

⁴Department of Surgery

Geffen School of Medicine, University of California, Los Angeles, Los Angeles, CA 90095, USA

⁵Department of Pathology, New York University School of Medicine, Bellevue Hospital Center, New York, NY 10016, USA

⁶Department of Pathology, Genentech Incorporated, South San Francisco, CA 94080, USA

*Correspondence: lowe@cshl.edu (S.W.L.), powers@cshl.edu (S.P.)

DOI 10.1016/j.ccr.2011.01.040

SUMMARY

We screened 124 genes that are amplified in human hepatocellular carcinoma (HCC) using a mouse hepatoblast model and identified 18 tumor-promoting genes, including *CCND1* and its neighbor on 11q13.3, *FGF19*. Although it is widely assumed that *CCND1* is the main driving oncogene of this common amplicon (15% frequency in HCC), both forward-transformation assays and RNAi-mediated inhibition in human HCC cells established that *FGF19* is an equally important driver gene in HCC. Furthermore, clonal growth and tumorigenicity of HCC cells harboring the 11q13.3 amplicon were selectively inhibited by RNAi-mediated knockdown of *CCND1* or *FGF19*, as well as by an anti-FGF19 antibody. These results show that 11q13.3 amplification could be an effective biomarker for patients most likely to respond to anti-FGF19 therapy.

INTRODUCTION

Developing cancer therapeutic strategies is particularly important in human hepatocellular carcinoma (HCC), which has limited treatment options and generally poor prognosis (Minguez et al., 2009). One concept for identifying strategies is oncogene dependence, in which tumor cells become overly dependent on a single activated oncogene for their sustained proliferation or survival (Weinstein and Joe, 2008). One of the best-described cases of oncogene dependence with corresponding therapeutic efficacy is *HER2* amplification in breast cancers (Faber et al., 2010). This argues that the wealth of genomic information that now exists regarding gene amplification in cancer could be used to find additional oncogene dependencies. However, numerous passenger genes are coamplified with the tumor-promoting driver genes, which complicates driver gene identification (Albertson et al., 2003). Currently, the only genome-wide

approaches to amplified driver gene identification are computational (Beroukhi et al., 2010; Woo et al., 2009).

The primary goal of this study was to develop a genome-wide functional approach that could assess, in an appropriate genetic and physiological context, the oncogenicity of candidate driver genes from amplicons found in human HCC. Our second goal was to determine if a specific driver gene amplification with a corresponding oncogene dependency could pinpoint a therapeutic strategy for HCC.

RESULTS

Identification and Functional Validation of Focal Amplicons in Human HCC

To identify regions of recurrent amplification in human HCC, we measured copy number alterations in 89 primary HCCs of different etiologies (hepatitis B, hepatitis C, or ethyl-toxic liver

Significance

Hepatocellular carcinoma (HCC) afflicts more than 560,000 people worldwide each year and has one of the worst 1-year survival rates of any cancer type. Currently, there are no molecular therapies that target specific mutations or other genetic alterations in HCC. By performing a forward-genetic screen guided by genomic analysis of human HCC, and through subsequent analysis with mouse models and RNAi, we found that a common genetic alteration in HCC (11q13.3 amplification) results in activation of *FGF19* and that this activation results in selective sensitivity to FGF19 inhibition. Our study underscores the potential for clinical translation of results obtained from genetic screens guided by cancer genome analysis.

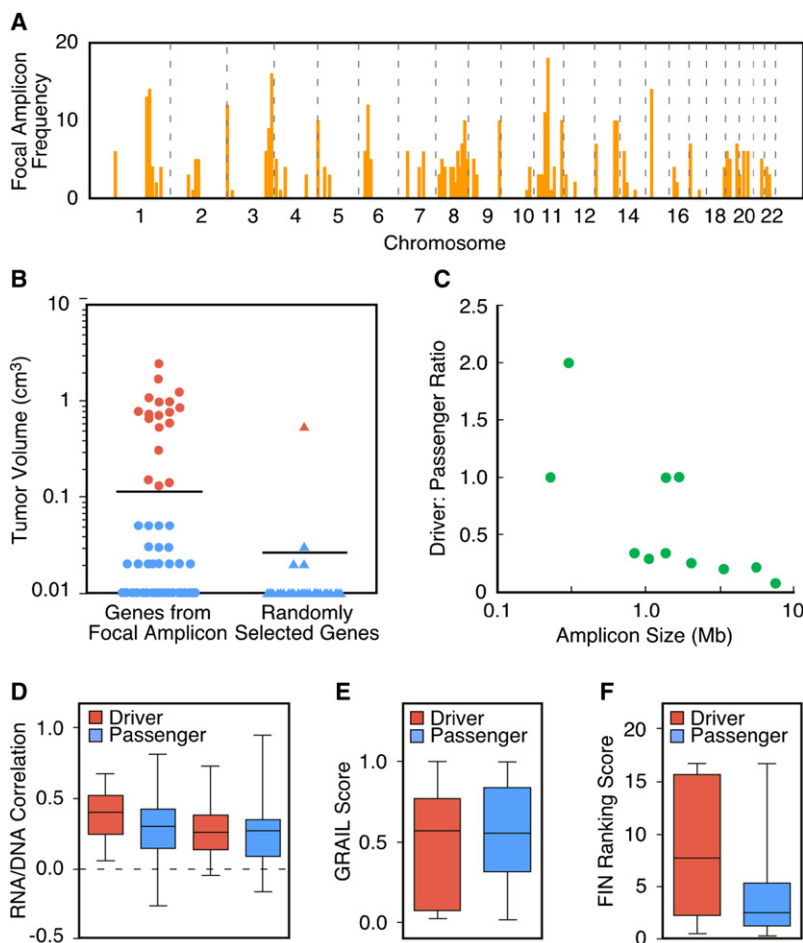


Figure 1. Recurrent Focal Amplicons in HCC Are Enriched for Tumor-Promoting Driver Genes

(A) Genome-wide frequency plot of focal amplicons (<10 Mb) identified by ROMA aCGH in 89 primary HCCs and 12 HCC cell lines.

(B) Comparison of the tumorigenicity induced by genes (cDNAs) picked from focal amplicons to randomly selected genes. p53^{-/-};Myc hepatoblasts transfected with cDNA expression constructs were injected subcutaneously, and after 42 days the resultant tumors were measured. Genes were scored as positive (red) if at least half the tumors measured greater than 0.1 cm³. Confirmation of tumorigenicity was performed as described in [Supplemental Experimental Procedures](#).

(C) The ratio of functionally validated drivers to passengers is displayed relative to the size of the amplicon in which the tested genes were located. Amplicon size was inversely correlated with the proportion of driver genes ($r = -0.70$; $p = 0.006$).

(D) Correlation coefficients of RNA levels to DNA copy number in two independent data sets are shown for both the driver and passenger genes. The two leftmost columns are from the data set reported here, and although the mean correlation was higher in the oncogenic set, it failed to pass the significance level of $p < 0.05$. The two rightmost columns are from the data set of [Chiang et al. \(2008\)](#).

(E) GRAIL scores of both the driver and passenger genes. The passenger genes have a very slightly lower mean GRAIL score, but this difference is not significant.

(F) FIN-based ranking scores of both the driver and passenger genes. The driver genes have a significantly higher mean value ($p < 0.018$). See also [Figure S2](#).

cirrhosis) and 12 HCC cell lines using the Representational Oligonucleotide Microarray Analysis (ROMA) array comparative genome hybridization platform. We selected amplified genes that were present in recurrent focal amplicons ([Figure 1A](#)) based on our hypothesis that genes within smaller amplicons are more likely to be tumor-promoting than those from larger chromosomal alterations. Early studies with amplified genes *N-MYC* and *ERBB2/HER2* established that gene amplification results in overexpression and that overexpressing corresponding cDNAs in an appropriate nonmalignant cell can be used to recapitulate tumor-promoting function ([Hudziak et al., 1987](#); [Schwab et al., 1985](#)). Based on this premise, we constructed a focused cDNA expression library that corresponded to genes within focal amplicons in HCC, so that by forced overexpression in an appropriate nonmalignant cell, we could determine tumor-promoting function. From the set of amplified genes within 29 recurrent focal amplicons, we constructed a retroviral expression library of 124 full-length cDNAs (see [Figure S1](#) available online). The selection of these 124 cDNAs was based solely on their availability from the Mammalian Gene Collection (MGC) at the time this project was initiated, and because many cDNAs were not available, we could not be comprehensive in terms of coverage for each of the 29 amplicons. To determine whether targeting genes from this oncogenomic set was more

effective than targeting those not selected based on any physical location in the genome, we constructed a parallel library of 35 full-length cDNAs from randomly chosen protein-coding genes ([Figure S1](#)).

We introduced these 159 cDNAs in pools into an immortalized line of embryonic hepatoblasts lacking p53 and overexpressing Myc that were not tumorigenic in vivo ([Zender et al., 2005](#)) and assessed their ability to promote tumorigenesis following transplantation into recipient mice. Of note, this is a relevant genetic context in which to assay candidate HCC tumor-promoting genes because more than 40% of all human HCCs overexpress *MYC*, and many harbor *p53* mutations or deletions ([Teufel et al., 2007](#)). Thus, these cells provide a “sensitized” background where a single additional lesion can trigger tumorigenesis. After testing the pooled cDNAs for their tumor-promoting activity, we validated each positive hit individually. A total of 18 of the 124 amplified genes were validated as tumor-promoting genes ([Table 1](#)), whereas only one out of the 35 randomly chosen genes promoted tumor formation, a statistically significant enrichment ($p < 0.001$) ([Figure 1B](#)). We also examined the relationship between amplicon size and the ratio of tested genes that promoted tumor formation (driver genes) versus those that did not (passenger genes). As predicted, we found that the smaller the amplicon size, the more likely that an individual gene within

Table 1. Tumor-Promoting Genes Identified by the Oncogenomic cDNA Screen

Tumor-Promoting Genes	Chromosomal Location ^a	Focal Amplicon Frequency ^b	Gain Frequency ^c	RNA/DNA Correlation ^d	Biochemical Function(s) ^e	Average Tumor Volume ^f
<i>FND3B</i> ^g	3q26.31	3%	19%	0.14	Unknown	0.59 ± 0.16
<i>IRF4</i>	6p25.3	6%	37%	0.21	Transcription factor	0.14 ± 0.04
<i>CLIC1</i>	6p21.33	3%	31%	0.29	Chloride channel	0.30 ± 0.11
<i>POLR1C</i> ^g	6p21.1	6%	32%	0.40	RNA Pol I and III subunit	0.15 ± 0.03
<i>MET</i>	7q31.2	3%	23%	0.40	Receptor tyrosine kinase	1.09 ± 0.23
<i>ZCCHC7</i> ^g	9p13.2	2%	9%	0.09	Unknown	0.72 ± 0.13
<i>MRPL41</i> ^g	9q34.3	5%	10%	0.46	Mitochondrial ribosomal protein	0.85 ± 0.19
<i>MRPS2</i> ^g	9q34.3	5%	10%	0.53	Mitochondrial ribosomal protein	0.13 ± 0.02
<i>PMPCA</i> ^g	9q34.3	5%	10%	0.50	Mitochondrial peptidase	1.23 ± 0.10
<i>RHOD</i> ^g	11q13.1	5%	12%	0.53	Rho GTPase	0.76 ± 0.18
<i>CCS</i> ^g	11q13.1	5%	12%	0.33	Copper chaperone	0.67 ± 0.061
<i>CCND1</i>	11q13.3	14%	20%	0.65	Activates CDK4/6 and ER	0.98 ± 0.33
<i>FGF19</i>	11q13.3	14%	20%	0.68	Ligand for FGFR4	0.53 ± 0.23
<i>CDK4</i>	12q14.1	3%	13%	0.25	Cell cycle serine kinase	2.43 ± 0.78
<i>TSPAN31</i> ^g	12q14.1	3%	13%	0.05	Unknown	0.71 ± 0.25
<i>HCK</i>	20q11.21	2%	34%	0.22	Src-like tyrosine kinase	1.70 ± 0.16
<i>POFUT1</i> ^g	20q11.21	2%	34%	0.27	Glycosyltransferase	0.78 ± 0.24
<i>PIM2</i>	Xp11.23	3%	17%	−0.10	Serine-threonine kinase	0.96 ± 0.41

Properties of the 18 genes (out of 124) that scored positive for tumorigenicity in the oncogenomic cDNA screen. See also Figure S1.

^aDetermined using the UCSC Genome Browser website.

^bRepresents the percentage of HCC samples that harbored a focal amplicon (<10 Mb) containing the specified gene.

^cRepresents the percentage of samples harboring either focal amplification or wider amplification.

^dThe Pearson's correlation coefficient of mRNA expression and DNA copy number was determined as described in the text.

^eBiochemical functions were obtained from literature searching.

^fThe mean tumor volume and standard error were determined using the subcutaneous assay (n = 8) as described in the text.

^gThe gene has not previously been reported to possess tumor-promoting activity.

it could promote tumor formation (Figure 1C). These results establish that focal amplicons in human HCC are enriched for tumor-promoting genes and that they were likely caused by genetic events that provided a selective advantage to the evolving HCC cell.

Because our screen functionally classified the 124 amplified genes into drivers and passengers, this provides an opportunity to rigorously test computational filters for their ability to predict tumor-promoting function. There are two such filters that have been used in computationally oriented driver gene predictions: the association of RNA expression with amplification (Woo et al., 2009); and GRAIL (Beroukhi et al., 2010), an algorithm that looks for related genes in the set of affected loci. Neither of these found a significant difference between the two sets (Figures 1D and 1E). The result from the former test indicates that the effects of DNA copy number on the expression of driver genes and passenger genes are relatively comparable. We also used functional enrichment tools to find subgroups of genes within our total list of 124 candidates that were significantly over-represented for gene ontology (GO) terms, pathways, and other functional categories. We then tested whether the identified subgroups were biased for either subset, but we found no significant bias.

Finally, we tested a newly developed functional interaction network (FIN) (Wu et al., 2010a). Each of the 124 genes was mapped to the network, and its cancer relevance was estimated by

a ranking system (<http://cbio.mskcc.org/tcga-generanker/>) that took into account all of its interacting genes. There was a highly significant difference in the FIN-based ranking scores for tumor-promoting genes compared to inactive genes (Figure 1F), and this corresponded with an ability to predict tumor-promoting function with high accuracy and reasonable specificity and sensitivity (Figure S2).

Several well-established oncogenes previously implicated in liver cancer were discovered by our screen, including *CCND1* and *MET* (Deane et al., 2001; Wang et al., 2001). *MET* encodes a receptor tyrosine kinase that has been shown to be biochemically activated in HCC (Wang et al., 2001), but it has not previously been shown to be genetically altered in human HCC. Inhibitors of c-met signaling in HCCs are being clinically tested (Gordon et al., 2010); our results would suggest that, rather than testing all patients with HCC, amplification and corresponding overexpression of *MET* (affecting up to 23% of patients; Table 1) may pinpoint a more responsive patient subgroup. Our results also suggest that small molecule inhibitors of the previously described oncogenes CDK4 and PIM2 be considered for targeted therapeutic development in HCC. The serine/threonine kinase oncogene *PIM2* plays a key role in survival signaling in hematopoietic cells (Fox et al., 2003). It has recently been shown to be overexpressed in human HCC and to be important for survival of the HCC cell line HepG2 (Gong et al., 2009).

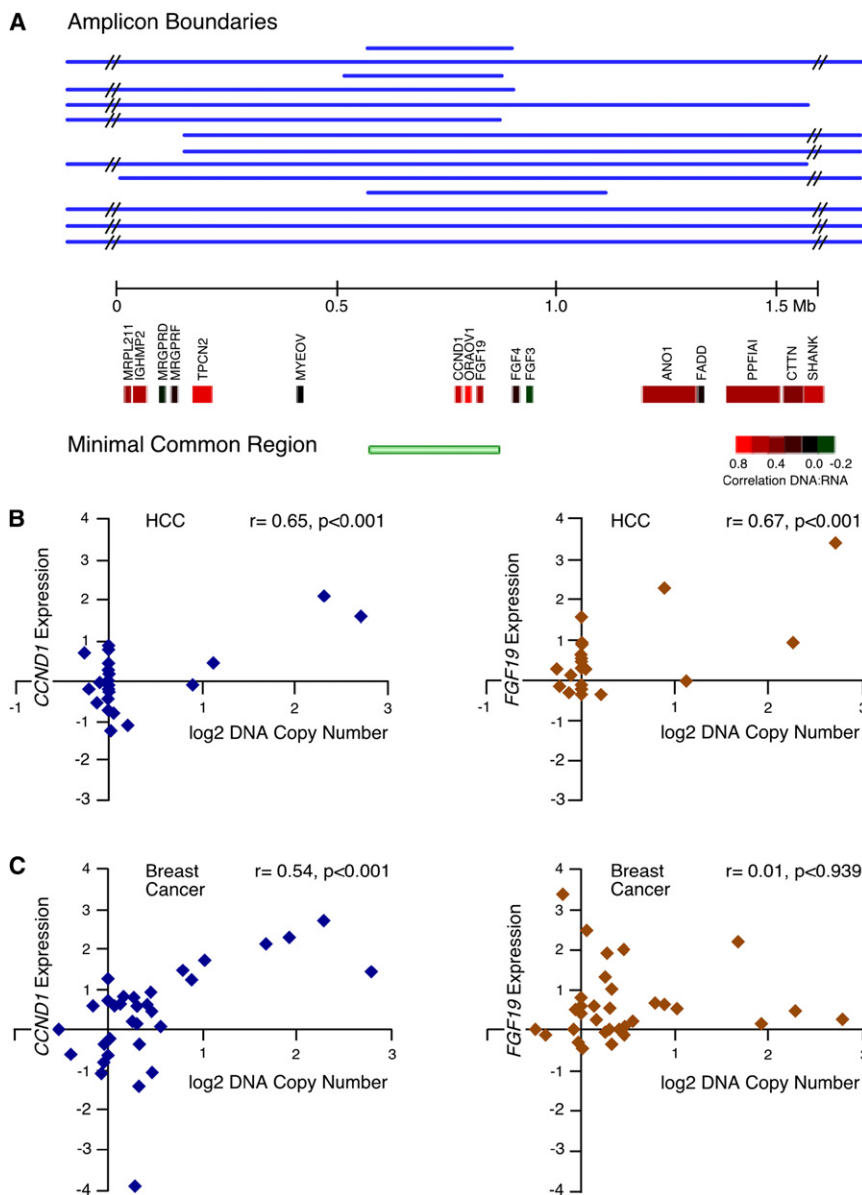


Figure 2. Epicenter Mapping and Expression of Genes in the 11q13.3 Amplicon in HCC and the Difference in the Effect of Amplification on *FGF19* and *CCND1* Expression between Breast and Liver Tumors

(A) Individual boundaries and the region of common overlap for the 14 11q13.3 amplicons, along with the underlying RefSeq genes in the depicted 1.5 Mb region, are displayed. The genes are color coded (see inserted scale) to indicate the degree of correlation between DNA copy number and gene expression. Correlation coefficients between DNA copy number and expression are for *FGF3* ($r = -0.20$; $p = 0.36$) and *FGF4* ($r = 0.17$; $p = 0.45$), statistically insignificant in HCC.

(B) Scatter plots with associated correlation coefficients showing the relationship in HCC samples (both tumors and cell lines) between DNA copy number and expression for *CCND1* (left) and *FGF19* (right).

(C) As in (B) but with breast cancer cell line samples. See also Figure S3.

ZCCHC7), and three are nuclear-encoded mitochondrial proteins (*MRPL41*, *MRPS2*, and *PMPCA*) (Table 1). It is possible that the latter three genes play a role in the mitochondrial apoptosis pathway. Finally, the tumor-promoting gene *POLR1C* encodes the highly conserved RPA40 subunit of both RNA Pol I and RNA Pol III. Its function can be characterized as “housekeeping” and is not associated with known signaling pathways involved in cancer. However, it has long been known that there is increased Pol I and Pol III transcription in cancer cells (White, 2008). Our results would suggest that this increase may actively drive cancer progression as opposed to it being a passive secondary event. Interestingly, RPA40 was shown recently to be tyrosine phosphorylated

(Rush et al., 2005), and this may provide another avenue for its activation in cancer.

***FGF19* and *CCND1* Are Both Overexpressed in HCCs Harboring the 11q13.3 Amplicon**

The 11q13.3 amplicon containing *CCND1* is one of the most frequent amplification events in human tumors and is well characterized; thus, it was surprising to find another tumor-promoting gene (*FGF19*) in the same region. *FGF19* lies within 45 kb of *CCND1*, and the two genes are invariably coamplified in the samples we analyzed, leading to an increase in expression of both genes (Figure 2A). *FGF4* and *FGF3* are also frequently coamplified with *CCND1*, though they are further away than *FGF19* (120 and 155 kb, respectively). However, *CCND1* and *FGF19* are often amplified in the absence of coamplification with these two other FGF genes (Figure 2A). Furthermore, we

Other genes that were identified in our screen include: *CLIC1*, which encodes an ion channel initially identified in a screen for genes involved in anchorage-independent growth of human HCC cell lines (Huang et al., 2004); *POFUT1*, a gene that encodes a glycosyltransferase that modifies Notch receptors (Stahl et al., 2008); *CCS*, a gene encoding a copper chaperone that is required for the activation of superoxide dismutase and helps protect cells from oxidative stress and cell death (Leitch et al., 2009; Matthews et al., 2000); *TSPAN31*, a member of the tetraspanin family of cell surface receptors, some of which have previously been linked to cancer (Hemler, 2008); and *RHOD*, a member of the Rho GTPase family that is involved in endosome motility and the localization of certain Src-kinase family members (Sandilands et al., 2007) (Table 1). The remaining six identified genes could not be readily linked to carcinogenesis. Two have unknown biochemical functions (*FNDC3B* and

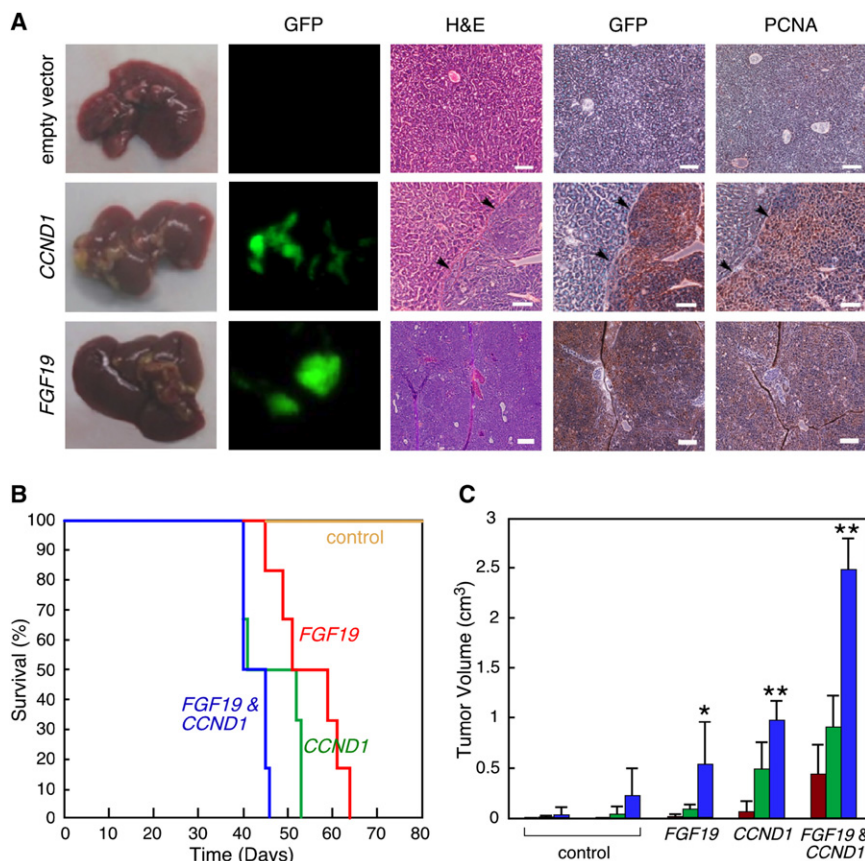


Figure 3. *FGF19* and *CCND1* Cooperate to Promote Liver Carcinoma Formation

(A) Images of mouse livers and liver sections taken 8 weeks following transplantation of $p53^{-/-}$;Myc hepatoblasts expressing empty vector, *CCND1*, or *FGF19*. The five panel columns are, from left to right: intact livers; fluorescent imaging of intact liver for GFP-positive transplanted cells; hematoxylin and eosin staining of liver tissue sections showing the border between normal liver and carcinoma (arrowheads); immunohistochemical detection of GFP; and immunohistochemical detection of PCNA. The last three are from the same tissue block. Scale bars, 100 μ m.

(B) Kaplan-Meier plot showing the percentage of mouse survival at various times after transplantation. The livers of mice were transplanted with $p53^{-/-}$;Myc hepatoblasts infected with control vectors, *FGF19* alone, *CCND1* alone, or both genes in combination.

(C) Subcutaneous growth of $p53^{-/-}$;Myc hepatoblasts infected with control vector pMSCVpuro, control vector pMSCVhygro, *FGF19* alone, *CCND1* alone, or *FGF19* with *CCND1* ($n = 10$ injections). Asterisks indicate that the indicated tumor group is significantly different than controls. Error bars denote \pm SD. * $p < 0.05$, ** $p < 0.0005$. Tumor volumes were determined on 28 (red columns), 35 (green columns), and 42 (blue columns) days after injection. See also Figure S4.

found that although amplification results in significant increases in *CCND1* and *FGF19* expression in HCC, amplification of *FGF4* and *FGF3* does not correlate with increased gene expression (Figures 2A and 2B). This lack of correlation of amplification and overexpression for these latter two FGF genes was previously noted in breast cancer (Fantl et al., 1990).

Curiously, the only report in the literature regarding the effect of amplification of *FGF19* on its expression was a study in oral cancer, where it was found to not be overexpressed despite gene amplification (Huang et al., 2006). Largely because *FGF19* was discovered after analyses of the 11q13.3 amplicon in breast cancer were conducted, there are no reports in the literature regarding the effect of amplification on its expression in breast cancer. We have found that, similar to oral cancer, *FGF19* is not overexpressed when amplified in breast cancer (Figures 2C; Figure S3), nor does *FGF19* appear to be overexpressed when amplified in lung cancer or melanoma (Figure S3). Thus, amplification does not invariably cause overexpression of *FGF19*; rather, overexpression appears restricted to a specific tissue type. We have previously reported this same phenomenon for the amplified gene *TTF1*, which is overexpressed when amplified in lung adenocarcinomas, but not in lung squamous carcinomas (Kendall et al., 2007).

ORAOV1, which is located between *FGF19* and *CCND1* (Figure 2A), is overexpressed in all amplified tumors that have been tested, including in our HCC data set. However, our screening showed that it does not promote tumorigenicity in

$p53^{-/-}$;Myc hepatoblasts, nor does it show any cooperativity with *FGF19* or *CCND1* (data not shown).

Effects of *FGF19* and *CCND1* Overexpression on Hepatocellular Tumorigenicity

We wanted to confirm that both *FGF19* and *CCND1* could induce tumorigenicity using an orthotopic transplantation assay. When hepatocytes overexpressing either *FGF19* or *CCND1* were transplanted into the liver of mice, tumors developed within 8 weeks (Figure 3A). Microscopic examination of the resultant in situ liver tumors classified them as aggressive solid HCCs. The tumors were composed of a population of undifferentiated cells growing as a sheet without any histological evidence for gland formation or any other structure. The cells were large with a more basophilic-staining cytoplasm compared to normal liver and resembled human HCC. We established that the tumors arose from the transfected hepatoblasts because the carcinoma cells were positive for the GFP marker. In addition, cellular proliferative status was examined by immunohistochemical staining for PCNA. The tumors formed by either *FGF19* or *CCND1*-expressing hepatoblasts were clearly positive for PCNA as well, indicating that the tumors induced by these genes were significantly proliferative. Similar morphological and molecular changes were observed in orthotopic tumors induced by *MET*, *POFUT1*, or *HCK* (Figure S4).

Next, we explored for possible cooperative effects when both *FGF19* and *CCND1* genes were coexpressed in murine

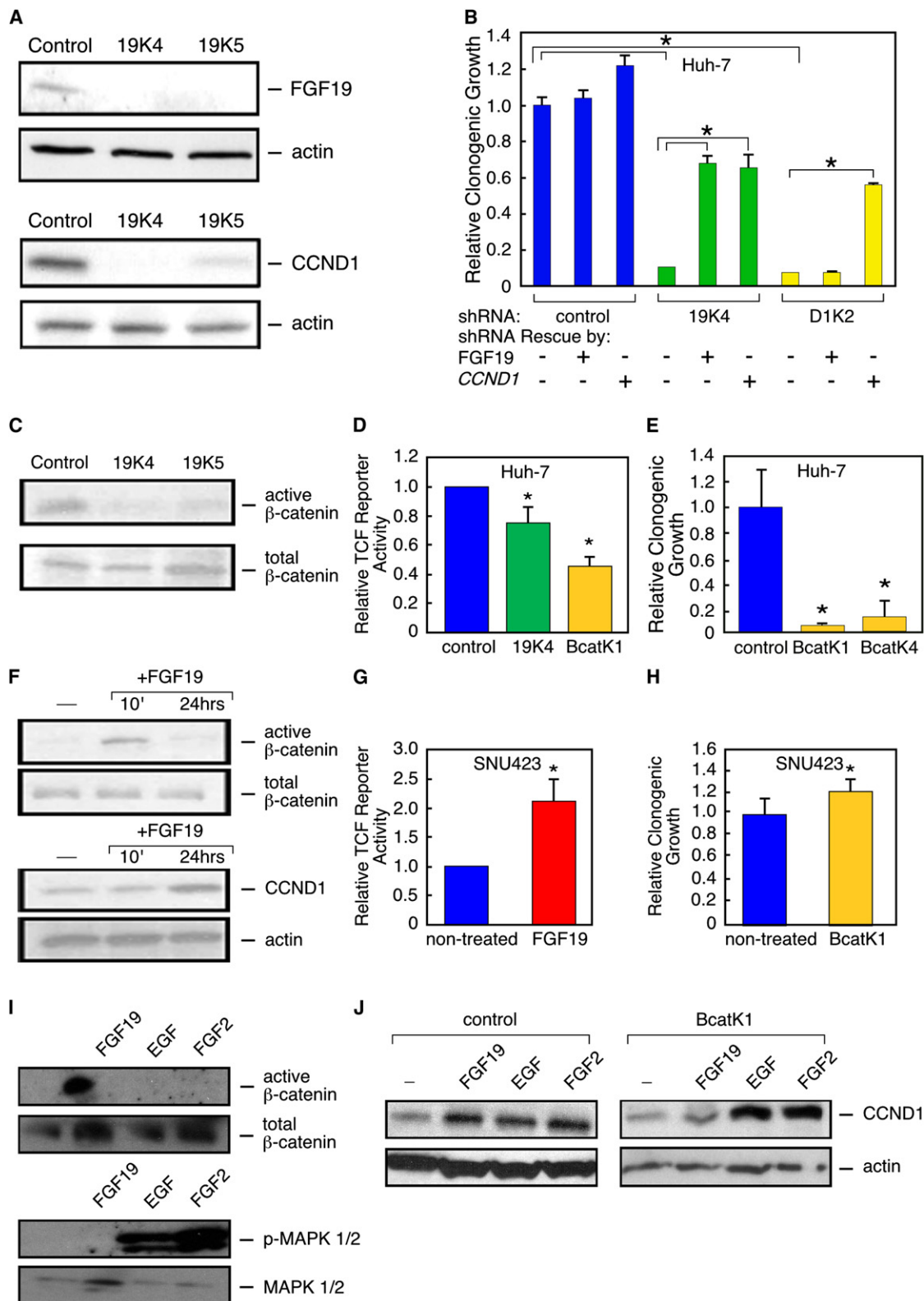


Figure 4. FGF19 and CCND1 Functionally Interact through β -Catenin Signaling

(A) FGF19 and cyclin D1 protein expression in Huh-7 (11q13.3-amplified) cells following stable transfection with one shRNA targeting luciferase (control) and two independent shRNAs targeting *FGF19* (19K4 and 19K5).

hepatoblasts. For the transplantation assays we measured the survival of mice transplanted with $p53^{-/-}$;Myc hepatoblasts ectopically expressing the two genes alone and also in combination. None of the control mice transplanted with hepatoblasts transfected with empty vectors died within the 100-day observation period, but 100% of the *FGF19* alone, *CCND1* alone, and *CCND1* plus *FGF19* groups did eventually succumb to tumors (Figure 3B). According to the log rank test for significance, the survival of the *FGF19* or *CCND1* alone and *CCND1* plus *FGF19* groups was significantly less than control ($p < 0.05$). There was an increase in morbidity when comparing the *CCND1* plus *FGF19* group to the *FGF19* or *CCND1* alone groups (Figure 3B). This difference was clearly significant when compared to the *FGF19* group alone ($p = 0.003$), but the difference compared with the *CCND1* alone group did not pass the $p = 0.05$ cutoff normally used for significance, although the p value obtained indicates only a 15% chance that the null hypothesis was correct ($p = 0.15$). In the subcutaneous tumorigenicity assay, which uses tumor volume as a readout, therefore providing a greater range of quantitative values than survival, the combination of both *CCND1* and *FGF19* was very clearly significantly greater than either gene alone ($p < 0.0005$; Figure 3C). Taken together, these results suggest that the combination of overexpressing *CCND1* and *FGF19* is more tumorigenic than when either single gene is overexpressed.

FGF19 Requires β -Catenin to Mediate Cyclin D1 Protein Levels

Because many growth factors are known to regulate cyclin D1 protein production, we wanted to determine whether *FGF19* levels in turn regulated cyclin D1 levels in human HCC cells. Toward this end, we tested and validated two shRNAs targeting *FGF19* and two shRNAs targeting *CCND1* that were each effective at reducing target protein levels (Figure S5). We found that RNAi-mediated silencing of *FGF19* in the HCC cell line Huh-7, which harbors the 11q13.3 amplicon and overexpresses both *FGF19* and *CCND1* (Figure S5), caused what appeared to be complete suppression of FGF19 protein as well as almost complete elimination of cyclin D1 protein (Figure 4A). Furthermore, we found that silencing the expression of either *FGF19*

or *CCND1* significantly inhibited clonogenic growth of Huh-7 cells (Figure 4B). To control for off target effects of the shRNAs, we performed RNAi rescue experiments. We found that the addition of recombinant FGF19 protein to the culture medium restored high levels of cyclin D1 protein and rescued the growth defect caused by shRNA knockdown of *FGF19* but that it could not do either to cells with the shRNA knockdown of *CCND1* (Figures 4B; Figure S5). On the other hand, overexpression of an RNAi-insensitive *CCND1* construct restored high levels of cyclin D1 protein and completely rescued the growth defects of both *FGF19* and *CCND1* shRNA knockdowns (Figures 4B; Figure S5). These results show that the shRNA effects were not off target, and they also establish a clear hierarchy of onco-gene dependence, in that FGF19 functions upstream of cyclin D1 in human HCC cells.

We aimed to identify a potential mechanism through which FGF19 is regulating cyclin D1 levels. Recently, one of us (D.M.F.) showed that in colon cancer cell lines, expression of *FGF19* activates β -catenin signaling, whereas its inhibition reduces β -catenin signaling (Pai et al., 2008). β -Catenin has been proposed to activate *CCND1* transcription (Tetsu and McCormick, 1999), although it is not always an immediate transcriptional target (Sansom et al., 2005), and it can also influence cyclin D1 levels by stabilization of *CCND1* mRNA (Briata et al., 2003). This led us to predict that FGF19 may be signaling through β -catenin to regulate cyclin D1 protein levels. To test this we determined if the knock down of *FGF19* would have an effect on β -catenin activation. Levels of activated β -catenin protein were analyzed by immunoblotting using an antibody directed against NH₂-terminally dephosphorylated β -catenin. We found that both shRNAs targeting *FGF19* caused a clear reduction of β -catenin activation (Figure 4C). We wanted to determine if this held true if we used a dual-luciferase TCF reporter as a readout for β -catenin activity. We found that in the 11q13.3-amplified Huh-7 cell line, TCF reporter activity was reduced by 25% when *FGF19* was knocked down and that a shRNA targeting β -catenin (*CTNNB1*) reduced activity by 55% (Figure 4D).

We then used shRNAs targeting *CTNNB1* to determine if reducing β -catenin would have an effect on cell growth of the 11q13.3-amplified HCC cell line Huh-7. Two shRNAs targeting

(B) Quantification of clonogenicity of Huh-7 cells infected with shRNAs against *FGF19* (19K4) and *CCND1* (D1K2) are shown relative to results obtained with a shRNA against luciferase (control). Recombinant FGF19 protein was added to the medium, or a shRNA-insensitive *CCND1* expression construct was transfected into the cells, where indicated. Error bars denote \pm SD. * $p < 0.005$.

(C) Active β -catenin levels in Huh-7 cells expressing the two shRNAs targeting *FGF19*, as revealed by immunoblotting with an antibody specific for the activated form of β -catenin, relative to total β -catenin levels.

(D) TCF reporter activity, relative to constitutively expressing renilla luciferase activity, in Huh-7 cells infected with shRNAs against *FGF19* (19K4) or β -catenin (BcatK1), compared to a shRNA against luciferase (control). Error bars denote \pm SD. * $p < 0.05$.

(E) Quantification of clonogenicity of Huh-7 cells infected with shRNAs against *CTNNB1* (BcatK1 and BcatK4) is shown relative to a nontargeting shRNA (control). Error bars denote \pm SD. * $p < 0.05$.

(F) Time course effects of adding FGF19 to the medium of SNU423 cells (with a single copy of 11q13.3) on active β -catenin levels, as well as the effects of added FGF19 on cyclin D1 protein levels, as detected by immunoblotting.

(G) TCF reporter activity, relative to constitutively expressing renilla luciferase activity, in SNU423 cells treated for 24 hr with recombinant FGF19, compared to nontreated cells. Error bars denote \pm SD. * $p < 0.05$.

(H) Quantification of clonogenicity in SNU423 cells infected with an effective shRNA against *CTNNB1* (BcatK1), compared to cells infected with a nontargeting shRNA. Error bars denote \pm SD. $p = 0.169$.

(I) SNU423 cells were treated with FGF19, EGF, or FGF2. β -Catenin and MAPK activity were determined by immunoblotting after 15 min, whereas cyclin D1 protein was detected after 24-hr exposure.

(J) SNU423 cells infected with either a nontargeting shRNA (control) or an effective shRNA targeting β -catenin (BcatK1) were treated with FGF19, EGF, or FGF2 for 24 hr and then cyclin D1 protein levels were detected by immunoblotting. See also Figure S5.

CTNNB1 significantly reduced the clonogenic growth potential of Huh-7, as compared to cells expressing a nontargeting shRNA (Figures 4E; Figure S5). This effect was not seen in the nonamplified HCC cell line SNU423 (Figure 4H). This further supports our model that β -catenin signaling is critical in *FGF19*-amplified HCC cell lines.

Conversely, we added FGF19 to the culture medium of a HCC cell line (SNU423) that has the normal copy number of both *FGF19* and *CCND1* and that does not express detectable levels of FGF19 protein by immunoblotting (Figure S6). These cells were incubated in medium supplemented with FGF19, and β -catenin activity was analyzed both by immunoblotting for NH_2 -terminally dephosphorylated β -catenin and by measuring TCF reporter activity. As determined by immunoblotting, the addition of FGF19 induced activation of β -catenin within 10 min, and baseline levels returned within 24 hr (Figure 4F). Correspondingly, TCF reporter activity was increased 2.1-fold in the presence of recombinant FGF19 (Figure 4G). We found that cyclin D1 protein levels were subsequently elevated after 24 hr of exposure to exogenously added FGF19 (Figure 4F), supporting a mechanism by which FGF19 induces elevated cyclin D1 through β -catenin signaling.

Our proposed mechanism for how FGF19 induces higher levels of cyclin D1 protein differs from how other mitogens have been shown to increase cyclin D1 protein in fibroblasts, a mechanism that requires MAP kinase activation (Lavoie et al., 1996). To test if this was also true in human HCC cells, we treated serum-starved SNU423 cells with FGF19, FGF2 (basic FGF), or EGF for 15 min and then analyzed β -catenin and MAPK1/2 activation. We also treated the cells for 24 hr to measure cyclin D1 protein levels. We found that all three growth factors were able to induce elevation of cyclin D1 protein; however, only FGF19 activated β -catenin, whereas only EGF and FGF2 activated MAPK1/2 (Figure 4I). We also determined, using an effective shRNA against *CTNNB1*, that β -catenin function was selectively required by FGF19 to induce cyclin D1 but that this was not true for EGF or FGF2 (Figure 4J). We conclude that there are two distinct pathways in HCC cells through which mitogens induce elevation of cyclin D1 protein: the well-established pathway involving RAS/RAF/MAPK signaling, and the β -catenin pathway.

***CCND1* and *FGF19* Oncogene Dependency in Human HCC Cell Lines**

We wanted to test whether amplification of *CCND1* and *FGF19* in human HCC cell lines led to dependence on their continued expression and, if so, whether such oncogene dependence would hold true in HCC cell lines that were not amplified for 11q13.3. Toward this end we used the previously described shRNAs targeting *FGF19* and *CCND1* to test oncogene dependence in a panel of six HCC cell lines: three harboring amplification of 11q13.3, and three that were single copy for this locus. We introduced these shRNAs into each of the six cell lines and tested their effects on growth using a clonal growth assay. Strikingly, the clonogenic growth potential of each of the three *CCND1/FGF19*-amplified cell lines was significantly reduced by silencing of either *FGF19* or *CCND1*, whereas none of the *CCND1/FGF19* single-copy cell lines was significantly affected (Figures 5A and 5B). These results establish a clear link between

genotype (*CCND1/FGF19* copy number status) and oncogene dependence.

We wanted to determine if the selective inhibition of the 11q13.3-amplified tumor cells by shRNAs targeting either *FGF19* or *CCND1* was reflected in correspondingly different levels of expression of the gene products in untreated cells. We found that FGF19 protein could be detected in all three 11q13.3-amplified HCC cell lines, but none of the nonamplified cell lines (Figure S6), an expected result based on the notion that gene amplification drives increased mRNA and protein expression. However, cyclin D1 protein levels did not vary significantly between the two groups (Figure S6), which could be explained by the high levels of mitogens found in the cell culture conditions keeping cyclin D1 levels high, regardless of amplification status. However, this result indicates that the selective dependence of the 11q13.3-amplified cells for cyclin D1 is not due to addiction to higher levels of cyclin D1 protein but, rather, to selective dependence on cyclin D1 downstream effector functions.

We then tested whether elevated expression of these two genes in the *CCND1/FGF19*-amplified cell line Huh-7 played a significant role in vivo. The shRNAs silencing either *FGF19* or *CCND1* significantly slowed the growth of Huh-7 cells transplanted subcutaneously into nude mice ($p < 0.005$; Figure 5C). Significant inhibition of tumor growth by shRNAs targeting *FGF19* or *CCND1* was also observed with *CCND1/FGF19*-amplified JHH-7 cells ($p < 0.0001$; Figure 5D). These results establish key tumor maintenance functions for both *FGF19* and *CCND1* specifically in HCCs harboring the 11q13.3 amplicon, but not in those without.

Despite the fact that most cancers contain several oncogenic alterations affecting multiple genes, oncogene dependence has almost always been evaluated for only a single oncogene, although it has been shown that in some circumstances, inhibition of multiple altered oncogenes can be beneficial (Podsypanina et al., 2008). This led us to test whether shRNA-mediated silencing of both driver genes in the 11q13.3 amplicon would be more effective than silencing of *FGF19* or *CCND1* alone. To test this we coexpressed effective shRNAs against each gene in the 11q13.3-amplified JHH-7 line. By measuring clonogenic growth we found that the dual shRNA knockdown was no more effective in suppressing growth than shRNA knockdown of either gene alone (Figure S6). Nor did the dual shRNA knockdown show more effective inhibition of tumor development (Figure S6). We believe this result supports our model that the tumor-promoting effects of *FGF19* are mediated by its ability to increase cyclin D1 protein levels and that because single shRNAs targeting either *FGF19* or *CCND1* can effectively lower cyclin D1 protein levels (Figures 4A; Figure S5), additional lowering of cyclin D1 protein levels has no growth-inhibitory effect. However, we do not believe that this negative result should be extrapolated to other situations where driver genes may operate in different pathways.

A Neutralizing Anti-FGF19 Monoclonal Antibody Blocks Clonogenicity and Tumorigenicity of 11q13.3-Amplified HCCs

We next sought to test the potential benefit of targeting FGF19 therapeutically in 11q13.3-amplified HCCs. We assayed the

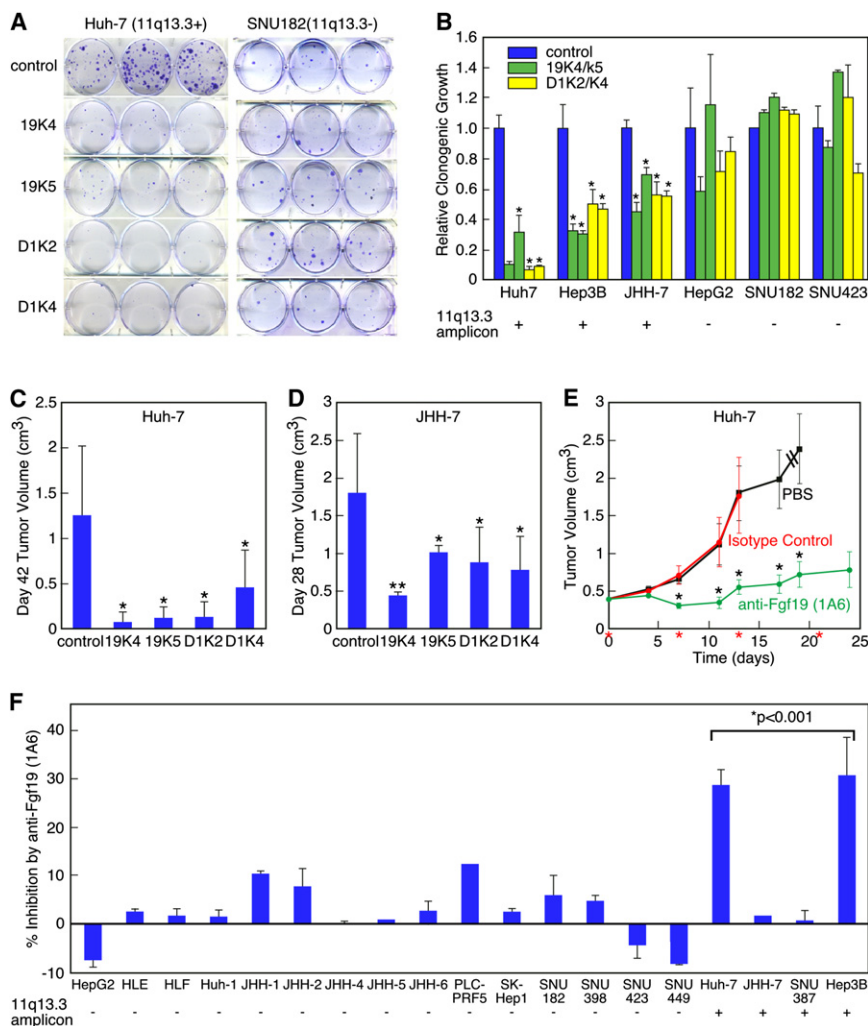


Figure 5. *CCND1* and *FGF19* Oncogene Dependency in Human HCC Cell Lines

(A) Clonogenicity assay of Huh-7 cells (11q13.3-amplified) and SNU182 cells (single copy for 11q13.3) infected with shRNAs against luciferase (control), *FGF19* (19K4 and 19K5), and *CCND1* (D1K2 and D1K4).

(B) Quantification of clonogenicity in six cell lines (three with 11q13.3 amplification and three without) infected with shRNAs against *FGF19* (19K4 and 19K5) and *CCND1* (D1K2 and D1K4) relative to a shRNA against luciferase (control). Results with cells infected with control shRNA are shown in blue, anti-*FGF19* results with 19K4 and 19K5 shRNAs are shown in green, and anti-*CCND1* results with D1K2 and D1K4 shRNAs are shown in yellow. Error bars denote \pm SD. * $p < 0.001$.

(C) Subcutaneous tumor growth in nude mice of Huh-7 cells infected with indicated shRNAs ($n = 12$ injections). Error bars denote \pm SD. * $p < 0.005$.

(D) As in (C) but with JHH-7 cells ($n = 10$ injections). Error bars denote \pm SD. * $p < 0.01$, ** $p < 0.0001$.

(E) Subcutaneous growth of established tumors from Huh-7 cells treated with PBS, control antibody, or anti-*FGF19* antibody (1A6). Treatment was on the days marked with red asterisks. Dashed lines indicate that mice were terminated before the end of the study ($n = 20$ injections). Error bars denote \pm SEM. * $p < 0.05$.

(F) Growth inhibition of HCC cell lines grown in vitro with anti-*FGF19* antibody (1A6) relative to the indicated 11q13.3 amplification status. Error bars denote \pm SEM. The bracket above the four amplified cell lines indicates that by Student's t test, the average growth inhibition by the anti-*FGF19* antibody was significantly greater than that of the nonamplified control group. See also Figure S6.

effect of neutralizing FGF19 on the tumor-forming ability of Huh-7 cells using a previously characterized neutralizing antibody specific against FGF19 (1A6) (Desnoyers et al., 2008). Mice were injected subcutaneously with Huh-7 cells, and tumors were allowed to reach a size of 0.2 cm³. At that point, mice were placed into three treatment groups: one injected intraperitoneally with PBS, another with an isotype-matched control antibody, and the final group with neutralizing antibody 1A6. Most of the animals from the PBS and isotype-matched control antibody groups were sacrificed when the tumor burden became excessive. However, the anti-*FGF19* antibody had a dramatic inhibitory effect on tumor growth (Figure 5E). This result highlights the potential of using an anti-*FGF19* monoclonal antibody as a therapeutic for HCC.

To test whether the inhibitory effect of the anti-*FGF19* monoclonal antibody was specific for *CCND1/FGF19*-amplified HCCs, we examined a panel of HCC cell lines with different 11q13.3 amplification status and measured the inhibitory effect of the anti-*FGF19* monoclonal antibody using a short-term in vitro growth assay. None of the 15 HCC cell lines that did

not harbor the 11q13.3 amplicon showed significant response to the neutralizing antibody 1A6, whereas two out of four of the *CCND1/FGF19*-amplified lines were clearly inhibited by the antibody (Figure 5F). The 50% response rate observed in amplified HCC cell lines is similar to what has been shown using the anti-*Her2/neu* monoclonal antibody trastuzumab in *HER2*-over-expressing breast cancer cell lines (Pegram et al., 1998). With the exception of JHH-7, these results correspond closely with the results obtained with RNAi: both showed that inhibition of FGF19 attenuates the growth of 11q13.3-amplified HCCs, but not nonamplified HCCs. The discrepancy with JHH-7 may be due to the considerably higher level of FGF19 produced in this cell line relative to other *CCND1/FGF19*-amplified cell lines, making it potentially more difficult for the antibody to neutralize sufficient FGF19 protein (Figure S6). Nevertheless, this investigation of the panel of HCC cell lines shows that amplification of *CCND1/FGF19* is an accurate predictor of growth inhibition in response to the neutralizing antibody 1A6. This would also suggest that testing antibodies to FGF19 in the clinic should be restricted to patients with 11q13.3-amplified HCCs.

DISCUSSION

In this report we have shown that it is possible to identify the underlying driver genes of human cancer amplicons by screening appropriately selected pools of cDNAs for their ability to promote tumorigenesis in a mosaic mouse model. Through more in-depth analysis of two of these tumor-promoting amplified genes, we established that *FGF19* is an oncogene that is coamplified and co-overexpressed with *CCND1* in HCC. We also demonstrated that by inhibition of FGF19 with RNAi or with a potentially therapeutic monoclonal antibody, one can block the clonal growth and tumorigenicity of human HCC cells harboring the *FGF19/CCND1* amplicon. Given that there are currently no genetically targeted therapies for HCC, we believe these results represent an important biomedical advance.

Previously, one of us (D.M.F.) showed that transgenic mice with *FGF19* expressed in the skeletal muscle eventually developed liver tumors through a poorly understood but presumably paracrine mechanism (Nicholes et al., 2002) and that an anti-FGF19 monoclonal antibody prevented tumor formation in this model in addition to inhibiting xenograft tumor formation of some human colon cancer cell lines (Desnoyers et al., 2008). However, these studies did not establish the basis for how *FGF19* was involved in human cancer, which clearly can involve a cell autonomous mechanism, nor did they provide a clear strategy for selecting a likely-to-respond subpopulation of patients for treatment with the monoclonal antibody.

It is not clear if there is a biological explanation for why *CCND1* and *FGF19* are invariably coamplified in HCC, or if their coamplification is a secondary consequence of their close proximity and a result of amplicon formation involving DNA breaks at specific regions (Gibcus et al., 2007). Nevertheless, our data indicate that the two genes are functionally linked in that cyclin D1 levels in hepatocytes are dependent upon FGF19 signaling. Additionally, although the downstream effector of FGF19 in hepatocytes and HCC cells has been clearly established as FGFR4 (Wu et al., 2010b; Pai et al., 2008), which downstream effectors are involved in cyclin D1 in HCC cells is not clear. Cyclin D1 activates CDK4/6 kinase, which in turn inactivates RB1 (Sherr, 1996). Genetic lesions affecting RB1 pathway members, including the tumor suppressor *p16/INK4A*, can be mutually exclusive in certain cancers (Sherr, 1996). However, in some cancers *CCND1* amplification frequently co-occurs with *p16/INK4A* loss (Okami et al., 1999). Protein analysis of human HCC tumors suggests that this could be true with HCC (Azechi et al., 2001), which implies that other proteins that cyclin D1 binds to and influences (e.g., MYB, STAT3, PPAR γ) (Knudsen, 2006) are involved in cyclin D1 oncogenic effects in HCC.

It is surprising that amplicons do not always have the same driver genes in different tumor types; there is a fundamental difference between the 11q13.3 amplicon in breast and liver cancers in that *FGF19* is clearly overexpressed as a result of amplification in liver cancer but is not so in breast cancer. Thus, driver genes can be tissue type dependent, making it important to obtain amplification and overexpression data for different tumor types, even in the case of well-validated oncogenes.

We are optimistic that forward-genetic screens can be used generally for genome-wide identification of oncogenic driver

genes from DNA amplifications or other activating alterations identified by human cancer genome profiling. Most importantly, by performing follow-up experiments using RNAi in human cancer cell lines or mouse models, it should be possible to identify more oncogene dependencies and therapeutic targets. A key point about amplified driver genes is that they provide an immediate biomarker for identifying the patients that might benefit from treatment.

EXPERIMENTAL PROCEDURES

Tumor Samples, Cell Lines, and Genomic Analysis

The 89 primary HCC samples were obtained with appropriate Institutional Review Board (IRB) or corresponding committee approval, and patient informed consent was given by the Cooperative Human Tissue Network (n = 37), Hannover Medical School in Germany (n = 27), and the University of Hong Kong (n = 25). All tumor samples were de-identified prior to transfer to CSHL for analysis; hence, the study using these samples is not considered human subject research under the U.S. Department of Human and Health Services regulations and related guidance (45CFR, Part 46). Genomic DNA was isolated using proteinase K and 0.5% SDS, and RNA was isolated by TRIzol as described previously (Mu et al., 2003). HCC cell lines were obtained from ATCC or Japanese Collection of Research Bioresources (JCRB) and grown in the culture medium recommended by the supplier. DNA copy number profiling for all primary tumor samples and most HCC cell lines was performed by ROMA, a form of comparative genomic hybridization described previously (Lucito et al., 2003). Gene expression profiling was performed with NimbleGen Gene Expression arrays.

Oncogenomic Selection of Genes/cDNAs from Focal Amplicons and Construction of the Amplicon-Focused and Randomly Selected cDNA Libraries

We selected high-level amplicons (segmented value ≥ 1.5) that were ≤ 20 Mb in size and applied an algorithm similar to the minimal common region (MCR) method to determine the region of common overlap (Tonon et al., 2005). This analysis resulted in 29 commonly amplified regions, ranging in size from 230 kb to 10 Mb, with a total of 812 RefSeq genes (Figure S1). Starting with genes from the smallest amplicon, we obtained from Open Biosystems, a distributor of plasmids from the MGC (Gerhard et al., 2004), all available (as of June 2007) human or murine cDNA expression plasmids in the pCMV-SPORT6 vector until we had reached our target screen size of 150 cDNAs.

Generation of Liver Carcinomas and Tumorigenicity Assays

All studies utilizing murine hepatoblasts and the human xenograft experiments involving shRNAs were approved by Cold Spring Harbor's Institutional Animal Care and Use Committee. The human xenograft experiments involving antibodies were approved by Genentech's Institutional Animal Care and Use Committee. Early-passage immortalized liver progenitor cells were transduced by retroviruses expressing single cDNAs. Two million cells were transplanted into livers of female nu/nu mice (6–8 weeks of age) by intrasplenic injection, or one million cells were injected subcutaneously on NCR nu/nu mice. For cDNA pools, immortalized liver progenitor cells were transduced individually with cDNAs and, following selection, pooled in equal numbers immediately prior to injection. Tumor progression was monitored by abdominal palpation and whole-body GFP imaging. Subcutaneous tumor volume was measured using a caliper and calculated as: $0.52 \times \text{length} \times \text{width}^2$. For tumorigenicity assessment of human HCC cell lines and their derivatives, 5 million HCC cells were resuspended in serum-free MEM and injected into the flanks of irradiated 4-week-old female nude mice. Tumor size was measured weekly by caliper and calculated as above. For the xenograft studies with the anti-FGF19 antibody, 5 million Huh-7 cells were resuspended in 50% HBSS and 50% Matrigel (BD Biosciences) and injected subcutaneously into nude mice. When tumors reached a mean volume of 0.2 cm^3 , the mice were randomized into groups with similar mean tumor volumes. The groups of mice were then treated intraperitoneally on the indicated days with PBS,

30 mg/kg of an isotype-matched control antibody, or 30 mg/kg of 1A6, an anti-FGF19 antibody previously characterized.

ACCESSION NUMBERS

The ROMA microarray data in this study can be freely accessed through NCBI (GSE22916).

SUPPLEMENTAL INFORMATION

Supplemental Information includes six figures and Supplemental Experimental Procedures and can be found with this article online at [doi:10.1016/j.ccr.2011.01.040](https://doi.org/10.1016/j.ccr.2011.01.040).

ACKNOWLEDGMENTS

We thank L. Bianco, J. Marchica, T. Wang, A. Bakleh, and Q. Liu for technical support, J. Duffy for his help preparing figures, and A. Ashkenazi for discussions. This work was supported by the Hope Funds for Cancer Research (E.T.S.), and NIH grants CA124648 (S.P.), CA105388 (S.P. and S.W.L.), and CA076905 (R.S.F.). S.W.L. is a Howard Hughes Investigator. R.S.F. is a recipient of an NIH-LRP award. E.T.S., S.P., and S.W.L. are members of the CSHL Cancer Target Discovery and Development Center (CTD², supported by CA148532) and part of the NCI CTD² Network.

Received: June 23, 2010

Revised: October 26, 2010

Accepted: January 14, 2011

Published: March 14, 2011

REFERENCES

- Albertson, D.G., Collins, C., McCormick, F., and Gray, J.W. (2003). Chromosome aberrations in solid tumors. *Nat. Genet.* **34**, 369–376.
- Azechi, H., Nishida, N., Fukuda, Y., Nishimura, T., Minata, M., Katsuma, H., Kuno, M., Ito, T., Komeda, T., Kita, R., et al. (2001). Disruption of the p16/cyclin D1/retinoblastoma protein pathway in the majority of human hepatocellular carcinomas. *Oncology* **60**, 346–354.
- Beroukhi, R., Mermel, C.H., Porter, D., Wei, G., Raychaudhuri, S., Donovan, J., Barretina, J., Boehm, J.S., Dobson, J., Urashima, M., et al. (2010). The landscape of somatic copy-number alteration across human cancers. *Nature* **463**, 899–905.
- Briata, P., Ilengo, C., Corte, G., Moroni, C., Rosenfeld, M.G., Chen, C.Y., and Gherzi, R. (2003). The Wnt/beta-catenin → Pitx2 pathway controls the turnover of Pitx2 and other unstable mRNAs. *Mol. Cell* **12**, 1201–1211.
- Chiang, D.Y., Villanueva, A., Hoshida, Y., Peix, J., Newell, P., Minguéz, B., LeBlanc, A.C., Donovan, D.J., Thung, S.N., Solé, M., et al. (2008). Focal gains of VEGFA and molecular classification of hepatocellular carcinoma. *Cancer Res.* **68**, 6779–6788.
- Deane, N.G., Parker, M.A., Aramandla, R., Diehl, L., Lee, W.J., Washington, M.K., Nanney, L.B., Shyr, Y., and Beauchamp, R.D. (2001). Hepatocellular carcinoma results from chronic cyclin D1 overexpression in transgenic mice. *Cancer Res.* **61**, 5389–5395.
- Desnoyers, L.R., Pai, R., Ferrando, R.E., Hotzel, K., Le, T., Ross, J., Carano, R., D'Souza, A., Qing, J., Mohtashemi, I., et al. (2008). Targeting FGF19 inhibits tumor growth in colon cancer xenograft and FGF19 transgenic hepatocellular carcinoma models. *Oncogene* **27**, 85–97.
- Faber, A.C., Wong, K.K., and Engelman, J.A. (2010). Differences underlying EGFR and HER2 oncogene addiction. *Cell Cycle* **9**, 851–852.
- Fantl, V., Richards, M.A., Smith, R., Lammie, G.A., Johnstone, G., Allen, D., Gregory, W., Peters, G., Dickson, C., and Barnes, D.M. (1990). Gene amplification on chromosome band 11q13 and oestrogen receptor status in breast cancer. *Eur. J. Cancer* **26**, 423–429.
- Fox, C.J., Hammerman, P.S., Cinalli, R.M., Master, S.R., Chodosh, L.A., and Thompson, C.B. (2003). The serine/threonine kinase Pim-2 is a transcriptionally regulated apoptotic inhibitor. *Genes Dev.* **17**, 1841–1854.
- Gerhard, D.S., Wagner, L., Feingold, E.A., Shenmen, C.M., Grouse, L.H., Schuler, G., Klein, S.L., Old, S., Rasooly, R., Good, P., et al. (2004). The status, quality, and expansion of the NIH full-length cDNA project: the Mammalian Gene Collection (MGC). *Genome Res.* **14**, 2121–2127.
- Gibcus, J.H., Kok, K., Menkema, L., Hermesen, M.A., Mastik, M., Kluin, P.M., van der Wal, J.E., and Schuurin, E. (2007). High-resolution mapping identifies a commonly amplified 11q13.3 region containing multiple genes flanked by segmental duplications. *Hum. Genet.* **121**, 187–201.
- Gong, J., Wang, J., Ren, K., Liu, C., Li, B., and Shi, Y. (2009). Serine/threonine kinase Pim-2 promotes liver tumorigenesis induction through mediating survival and preventing apoptosis of liver cell. *J. Surg. Res.* **153**, 17–22.
- Gordon, M.S., Sweeney, C.S., Mendelson, D.S., Eckhardt, S.G., Anderson, A., Beaupre, D.M., Branstetter, D., Burgess, T.L., Coxon, A., Deng, H., et al. (2010). Safety, pharmacokinetics, and pharmacodynamics of AMG 102, a fully human hepatocyte growth factor-neutralizing monoclonal antibody, in a first-in-human study of patients with advanced solid tumors. *Clin. Cancer Res.* **16**, 699–710.
- Hemler, M.E. (2008). Targeting of tetraspanin proteins—potential benefits and strategies. *Nat. Rev. Drug Discov.* **7**, 747–758.
- Huang, J.S., Chao, C.C., Su, T.L., Yeh, S.H., Chen, D.S., Chen, C.T., Chen, P.J., and Jou, Y.S. (2004). Diverse cellular transformation capability of overexpressed genes in human hepatocellular carcinoma. *Biochem. Biophys. Res. Commun.* **315**, 950–958.
- Huang, X., Godfrey, T.E., Gooding, W.E., McCarty, K.S., Jr., and Gollin, S.M. (2006). Comprehensive genome and transcriptome analysis of the 11q13 amplicon in human oral cancer and synteny to the 7F5 amplicon in murine oral carcinoma. *Genes Chromosomes Cancer* **45**, 1058–1069.
- Hudziak, R.M., Schlessinger, J., and Ullrich, A. (1987). Increased expression of the putative growth factor receptor p185HER2 causes transformation and tumorigenesis of NIH 3T3 cells. *Proc. Natl. Acad. Sci. USA* **84**, 7159–7163.
- Kendall, J., Liu, Q., Bakleh, A., Krasnitz, A., Nguyen, K.C., Lakshmi, B., Gerald, W.L., Powers, S., and Mu, D. (2007). Oncogenic cooperation and coamplification of developmental transcription factor genes in lung cancer. *Proc. Natl. Acad. Sci. USA* **104**, 16663–16668.
- Knudsen, K.E. (2006). The cyclin D1b splice variant: an old oncogene learns new tricks. *Cell Div.* **1**, 15.
- Lavoie, J.N., Rivard, N., L'Allemain, G., and Pouyssegur, J. (1996). A temporal and biochemical link between growth factor-activated MAP kinases, cyclin D1 induction and cell cycle entry. *Prog. Cell Cycle Res.* **2**, 49–58.
- Leitch, J.M., Yick, P.J., and Culotta, V.C. (2009). The right to choose: multiple pathways for activating copper, zinc superoxide dismutase. *J. Biol. Chem.* **284**, 24679–24683.
- Lucito, R., Healy, J., Alexander, J., Reiner, A., Esposito, D., Chi, M., Rodgers, L., Brady, A., Sebat, J., Troge, J., et al. (2003). Representational oligonucleotide microarray analysis: a high-resolution method to detect genome copy number variation. *Genome Res.* **13**, 2291–2305.
- Matthews, C.C., Figueiredo, D.M., Wollack, J.B., Fairweather, N.F., Dougan, G., Hallewell, R.A., Cadet, J.L., and Fishman, P.S. (2000). Protective effect of supplemental superoxide dismutase on survival of neuronal cells during starvation. Requirement for cytosolic distribution. *J. Mol. Neurosci.* **14**, 155–166.
- Minguéz, B., Tovar, V., Chiang, D., Villanueva, A., and Llovet, J.M. (2009). Pathogenesis of hepatocellular carcinoma and molecular therapies. *Curr. Opin. Gastroenterol.* **25**, 186–194.
- Mu, D., Chen, L., Zhang, X., See, L.H., Koch, C.M., Yen, C., Tong, J.J., Spiegel, L., Nguyen, K.C., Servoss, A., et al. (2003). Genomic amplification and oncogenic properties of the KCNK9 potassium channel gene. *Cancer Cell* **3**, 297–302.
- Nicholes, K., Guillet, S., Tomlinson, E., Hillan, K., Wright, B., Frantz, G.D., Pham, T.A., Dillard-Telm, L., Tsai, S.P., Stephan, J.P., et al. (2002). A mouse model of hepatocellular carcinoma: ectopic expression of fibroblast growth factor 19 in skeletal muscle of transgenic mice. *Am. J. Pathol.* **160**, 2295–2307.
- Okami, K., Reed, A.L., Cairns, P., Koch, W.M., Westra, W.H., Wehage, S., Jen, J., and Sidransky, D. (1999). Cyclin D1 amplification is independent of p16

- inactivation in head and neck squamous cell carcinoma. *Oncogene* 18, 3541–3545.
- Pai, R., Dunlap, D., Qing, J., Mohtashemi, I., Hotzel, K., and French, D.M. (2008). Inhibition of fibroblast growth factor 19 reduces tumor growth by modulating beta-catenin signaling. *Cancer Res.* 68, 5086–5095.
- Pegram, M.D., Pauletti, G., and Slamon, D.J. (1998). HER-2/neu as a predictive marker of response to breast cancer therapy. *Breast Cancer Res. Treat.* 52, 65–77.
- Podsypanina, K., Politi, K., Beverly, L.J., and Varmus, H.E. (2008). Oncogene cooperation in tumor maintenance and tumor recurrence in mouse mammary tumors induced by Myc and mutant Kras. *Proc. Natl. Acad. Sci. USA* 105, 5242–5247.
- Rush, J., Moritz, A., Lee, K.A., Guo, A., Goss, V.L., Spek, E.J., Zhang, H., Zha, X.M., Polakiewicz, R.D., and Comb, M.J. (2005). Immunoaffinity profiling of tyrosine phosphorylation in cancer cells. *Nat. Biotechnol.* 23, 94–101.
- Sandilands, E., Brunton, V.G., and Frame, M.C. (2007). The membrane targeting and spatial activation of Src, Yes and Fyn is influenced by palmitoylation and distinct RhoB/RhoD endosome requirements. *J. Cell Sci.* 120, 2555–2564.
- Sansom, O.J., Reed, K.R., van de Wetering, M., Muncan, V., Winton, D.J., Clevers, H., and Clarke, A.R. (2005). Cyclin D1 is not an immediate target of beta-catenin following Apc loss in the intestine. *J. Biol. Chem.* 280, 28463–28467.
- Schwab, M., Varmus, H.E., and Bishop, J.M. (1985). Human N-myc gene contributes to neoplastic transformation of mammalian cells in culture. *Nature* 316, 160–162.
- Sherr, C.J. (1996). Cancer cell cycles. *Science* 274, 1672–1677.
- Stahl, M., Uemura, K., Ge, C., Shi, S., Tashima, Y., and Stanley, P. (2008). Roles of Pofut1 and O-fucose in mammalian Notch signaling. *J. Biol. Chem.* 283, 13638–13651.
- Tetsu, O., and McCormick, F. (1999). Beta-catenin regulates expression of cyclin D1 in colon carcinoma cells. *Nature* 398, 422–426.
- Teufel, A., Staib, F., Kanzler, S., Weinmann, A., Schulze-Bergkamen, H., and Galle, P.R. (2007). Genetics of hepatocellular carcinoma. *World J. Gastroenterol.* 13, 2271–2282.
- Tonon, G., Wong, K.K., Maulik, G., Brennan, C., Feng, B., Zhang, Y., Khatry, D.B., Protopopov, A., You, M.J., Aguirre, A.J., et al. (2005). High-resolution genomic profiles of human lung cancer. *Proc. Natl. Acad. Sci. USA* 102, 9625–9630.
- Wang, R., Ferrell, L.D., Faouzi, S., Maher, J.J., and Bishop, J.M. (2001). Activation of the Met receptor by cell attachment induces and sustains hepatocellular carcinomas in transgenic mice. *J. Cell Biol.* 153, 1023–1034.
- Weinstein, I.B., and Joe, A. (2008). Oncogene addiction. *Cancer Res.* 68, 3077–3080.
- White, R.J. (2008). RNA polymerases I and III, non-coding RNAs and cancer. *Trends Genet.* 24, 622–629.
- Woo, H.G., Park, E.S., Lee, J.S., Lee, Y.H., Ishikawa, T., Kim, Y.J., and Thorgeirsson, S.S. (2009). Identification of potential driver genes in human liver carcinoma by genomewide screening. *Cancer Res.* 69, 4059–4066.
- Wu, G., Feng, X., and Stein, L. (2010a). A human functional protein interaction network and its application to cancer data analysis. *Genome Biol.* 11, R53.
- Wu, X., Ge, H., Lemon, B., Vonderfecht, S., Weiszmann, J., Hecht, R., Gupte, J., Hager, T., Wang, Z., Lindberg, R., et al. (2010b). FGF19-induced hepatocyte proliferation is mediated through FGFR4 activation. *J. Biol. Chem.* 285, 5165–5170.
- Zender, L., Xue, W., Cordon-Cardo, C., Hannon, G.J., Lucito, R., Powers, S., Flemming, P., Spector, M.S., and Lowe, S.W. (2005). Generation and analysis of genetically defined liver carcinomas derived from bipotential liver progenitors. *Cold Spring Harb. Symp. Quant. Biol.* 70, 251–261.